JOURNAL OF QUATERNARY SCIENCE (2008) **23**(6-7) 683–702

Published online in Wiley InterScience
(www.interscience.wiley.com) DOI: 10.1002/jqs.1195

Ages and inferred causes of Late Pleistocene glaciations on Mauna Kea, Hawai'i

JEFFREY S. PIGATI,[1†] MAREK ZREDA,[2*] CHRIS ZWECK,[2] PETER F. ALMASI,[2‡] DAVID ELMORE[3] and WARREN D. SHARP[4]
[1] University of Arizona Desert Laboratory, Tucson, Arizona, USA
[2] Department of Hydrology and Water Resources, University of Arizona, Tucson, Arizona, USA
[3] Department of Physics, Purdue University, West Lafayette, Indiana, USA
[4] Berkeley Geochronology Center, Berkeley, California, USA

Pigati, J. S., Zreda, M., Zweck, C., Almasi, P. F., Elmore, D. and Sharp, W. D. 2008. Ages and inferred causes of Late Pleistocene glaciations on Mauna Kea, Hawai'i. *J. Quaternary Sci.*, **Vol. 23** pp. 683–702. ISSN 0267-8179.

Received 27 August 2007; Revised 14 April 2008; Accepted 17 April 2008

ABSTRACT: Glacial landforms on Mauna Kea, Hawai'i, show that the summit area of the volcano was covered intermittently by ice caps during the Late Pleistocene. Cosmogenic ^{36}Cl dating of terminal moraines and other glacial landforms indicates that the last two ice caps, called Older Makanaka and Younger Makanaka, retreated from their maximum positions approximately 23 ka and 13 ka, respectively. The margins and equilibrium line altitudes of these ice caps on the remote, tropical Pacific island were nearly identical, which would seem to imply the same mechanism for ice growth. But modelling of glacier mass balance, combined with palaeotemperature proxy data from the subtropical North Pacific, suggests that the causes of the two glacial expansions may have been different. Older Makanaka air atop Mauna Kea was likely wetter than today and cold, whereas Younger Makanaka times were slightly warmer but significantly wetter than the previous glaciation. The modelled increase in precipitation rates atop Mauna Kea during the Late Pleistocene is consistent with that near sea level inferred from pollen data, which suggests that the additional precipitation was due to more frequent and/or intense tropical storms associated with eastward-moving cold fronts. These conditions were similar to modern La Niña (weak ENSO) conditions, but persisted for millennia rather than years. Increased precipitation rates and the resulting steeper temperature lapse rates created glacial conditions atop Mauna Kea in the absence of sufficient cooling at sea level, suggesting that if similar correlations existed elsewhere in the tropics, the precipitation-dependent lapse rates could reconcile the apparent difference between glacial-time cooling of the tropics at low and high altitudes.

KEYWORDS: cosmogenic ^{36}Cl; tropical glaciation; temperature lapse rate; positive degree day model (PDD); central Pacific.

Introduction

The last transition from glacial to interglacial conditions in the North Atlantic region was punctuated by multiple high-frequency climate oscillations (Heinrich, 1988; Bond and Lotti, 1995). While the timing of these oscillations is fairly well established, the spatial extent of their influence has remained uncertain (e.g. Denton and Hendy, 1994; Lowell *et al.*, 1995; Peteet, 1995; Singer *et al.*, 1998; Denton *et al.*, 1999; Newnham *et al.*, 1999). In the North Pacific, for example, continuous, high-resolution palaeoclimate records from the Santa Barbara Basin (Kennett and Ingram, 1995; Hendy *et al.*, 2002) clearly show that conditions along the coast were tightly coupled with the North Atlantic during the Late Pleistocene. Away from the coasts, however, evidence of such teleconnections is lacking. Marine sedimentation rates in the interior North Pacific are low, the deep waters are corrosive to calcium carbonate, and few opportunities exist to obtain terrestrial climate records (Lee and Slowey, 1999).

One exception is a sequence of glacial deposits near the summit of Mauna Kea, Hawai'i (19.8° N, 155.5° W, 4205 m above sea level (a.s.l.)), which contains information on the timing (age of glacial landforms) and magnitude (position of ice margins) of palaeoclimatic changes. Until recently, these glacial deposits had been difficult to date, and, consequently the chronology of glacial events on Mauna Kea was known only approximately (Porter *et al.*, 1977; Porter, 1979a,b; Dorn *et al.*, 1991; Wolfe *et al.*, 1997). In addition, because glaciers respond to a combination of climatic variables, primarily temperature and precipitation, multiple palaeoclimatic interpretations can be made from the same glacial record.

Here we report new measurements and analyse them together with existing palaeoclimatic data to solve both problems. First, we used cosmogenic ^{36}Cl surface-exposure

* Correspondence to: M. Zreda, Department of Hydrology and Water Resources, University of Arizona, Tucson, AZ 85721, USA.
E-mail: marek@hwr.arizona.edu
† Present address: US Geological Survey, Geologic Division, Denver Federal Center, Denver, Colorado, USA.
‡ Lamont-Doherty Earth Observatory of Columbia University, Palisades, New York, USA.

dating to develop a new chronology for moraines and other landforms associated with the last two glacial expansions on Mauna Kea. Then, we developed high-elevation temperature and precipitation estimates for the Makanaka glaciations that are based on a glacier mass balance model for Mauna Kea, our glacial chronology, a pollen-based record of air temperatures from the nearby island of O'ahu (Hotchkiss and Juvik, 1999), an alkenone-derived record of sea-surface temperatures (SSTs) from the subtropical North Pacific (Lee and Slowey, 1999; Lee *et al.*, 2001) and temperature lapse rates that include a new correction for atmospheric moisture. Finally, we analysed spatial patterns of precipitation during glacial times and speculate on the origin of moisture that caused precipitation sufficient to grow and maintain ice caps on Mauna Kea. Our results suggest that, although the maximum extents of the two Makanaka ice caps were similar, the climatic forcing mechanisms behind the glacial expansions may have been different.

Geological setting

Hawaii's highest volcano, Mauna Kea, has many distinctive features. But one stands out as truly extraordinary: the summit area was glaciated in the past, and today it is the only location in the interior tropical Pacific that exhibits unequivocal evidence of past glacial activity (Porter, 1979a). Glacial deposits and lava flows form a cap that conceals the underlying basalts of the volcano's shield stage, which ended more than 240 ka ago (Sharp *et al.*, 1996). The postshield cap consists of older basaltic lava flows of the Hamakua Volcanic Group, overlain by younger 'hawaiitic' lava flows of the Laupahoehoe Volcanic Group (Wolfe *et al.*, 1997). The Laupahoehoe group contains the Makanaka Glacial Member, the youngest known glacial unit on Mauna Kea, which is present as end moraines, lateral moraines and ground moraine that form a nearly continuous annulus between ~3400 and 3800 m a.s.l. (Fig. 1). Outwash channel deposits and at least one boulder-dominated outwash fan lay below the moraines.

The Makanaka glaciations were complex, with alternating advances and retreats of the glacier front that probably began during marine isotope stage (MIS) 3 and continued well into MIS 2 (Wolfe *et al.*, 1997; Porter, 2001; Blard *et al.*, 2007). It is not clear if these advances represented different glaciations that were separated by ice-free conditions at the summit or were simply multiple advances of the same body of ice. Preliminary cosmogenic ^{36}Cl surface-exposure ages for the Older Makanaka (18.3 ± 3.3 ka; 2σ; one moraine boulder), Younger Makanaka (17.4 ± 2.3 ka; 2σ; one moraine boulder), and a lava flow between the two Makanaka deposits (19.1 ± 3.0 ka; 2σ; one abraded bedrock sample) from the northwest flank of the volcano were statistically identical (Dorn *et al.*, 1991). (Note that these ^{36}Cl ages were recalculated from Dorn *et al.*, 1991, using production rates obtained with the software of Anderson *et al.*, 2007, based on the calibration dataset of Phillips *et al.*, 1996, 2001, and scaled in space and time using Desilets and Zreda, 2003). In another early cosmogenic dating study, Cerling and Craig (1994) reported cosmogenic ^{3}He results for two abraded bedrock samples from the south flank of the volcano that implied the summit area was free of ice by 11 ka ago (^{3}He ages were recalculated from Cerling and Craig, 1994, using scaling models of Desilets and Zreda, 2003, and Pigati and Lifton, 2004). Blard *et al.* (2007) recently reported cosmogenic ^{3}He ages for the Older Makanaka terminal moraine that ranged from 17.2 ± 1.7 ka to 19.1 ± 1.9 ka ($n = 3$) and three recessional moraines on the south flank of Mauna Kea that ranged between 14.5 ± 1.5 ka and 18.9 ± 1.9 ka BP ($n = 4$). Finally, radiocarbon ages from organic matter in sediments from Lake Waiau, a small lake formed in a volcanic crater at 3970 m a.s.l., indicate that the summit area was free of ice by 14.9 ± 1.3 ka (based on a ^{14}C age of 12.7 ± 0.9 ka (2σ) (Peng and King, 1992) and converted to calendar years using Calib v. 5.1.Beta (Stuiver and Reimer, 1993; Reimer *et al.*, 2004)).

Resolving the glacial chronology on Mauna Kea is especially important because the Hawaiian Islands are located >3500 km from any continental land mass and, therefore, Pleistocene ice caps responded to palaeoclimatic changes without complicating factors that can affect continental settings, such as the distance from open oceans, the presence of large topographic barriers that affect air movement and moisture transport, and the proximity to continental ice sheets that can influence local atmospheric circulation patterns. Moreover, the timing of ice cap expansion and retreat on Mauna Kea provides an important control point for palaeoclimate modelling and other studies that involve the central Pacific.

Methods

Cosmogenic ^{36}Cl chronology

We used *in situ* cosmogenic ^{36}Cl to determine surface exposure ages of boulders from moraines and other landforms associated with the Makanaka glaciations. *In situ* cosmogenic nuclides are produced in materials at the earth's surface by interactions of secondary cosmic ray particles (nucleons, muons) with target nuclei (Davis and Schaeffer, 1955; Lal, 1988). Once produced, these nuclides remain in place within the rock and accumulate predictably with time. Accumulation of *in situ* cosmogenic nuclides has been used to establish glacial chronologies in numerous settings (e.g. Phillips *et al.*, 1990; Gosse *et al.*, 1995), and the approach is considered reliable. Cosmogenic ^{36}Cl is produced in rocks mainly by spallation of ^{40}Ca and ^{39}K, neutron activation of ^{35}Cl, and, less importantly at high altitudes, by capture of slow muons by ^{40}Ca (Phillips *et al.*, 1986; Zreda *et al.*, 1991). If the nuclide production rates are known, measured concentrations of the nuclide can be used to determine how long rocks have been exposed to cosmic rays. In glacial settings, cosmogenic nuclides begin to accumulate in rocks exposed to cosmic rays by glacial retreat; thus, the initial time of exposure is contemporary with the onset of deglaciation that follows the maximum extent of an ice cap.

Field methods

We collected samples for cosmogenic ^{36}Cl dating from the tops of boulders using a hammer and chisel, keeping only the top few centimetres of each sample for analysis. Boulders were chosen for sampling based on their size, appearance and position on the landform. We evaluated hundreds of boulders from each landform for sampling, but found only a few at each location that we thought would yield reliable results. Suitable boulders from the Older Makanaka moraine were especially difficult to find; most were relatively small (<0.5 m in diameter) and did not project above the surrounding matrix by more than a few tens of centimetres. Where we did find suitable boulders for sampling, the crests of the Makanaka moraines were broad,

DOI: 10.1002/jqs

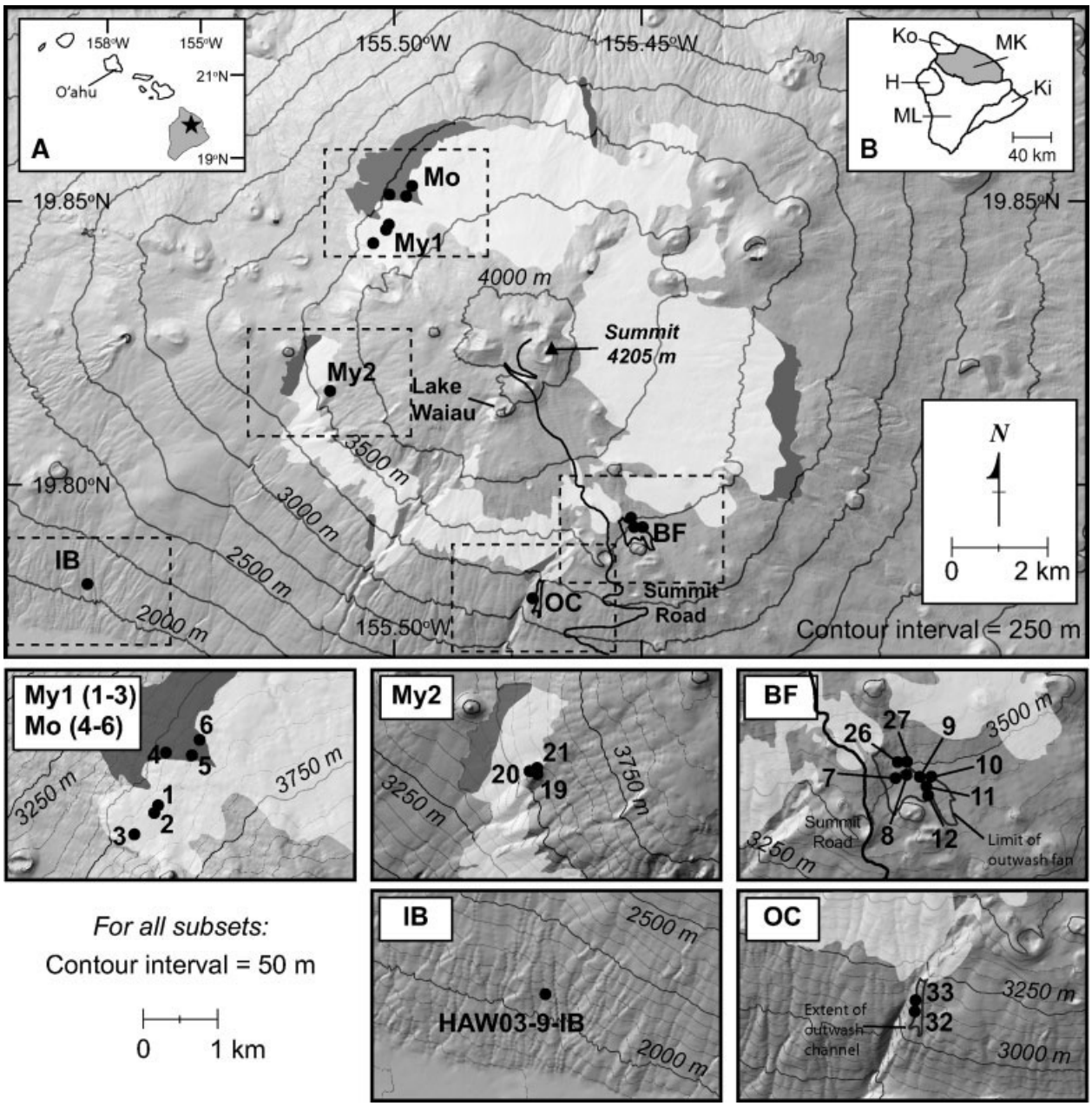

Figure 1 (A) Location of Hawaiian Islands (big island shaded; star denotes location of Mauna Kea). (B) Volcanoes of Hawai'i: H, Hualālai; Ki, Kilauea Ko, Kohala; MK, Mauna Kea (shaded); ML, Mauna Loa. (C) Location of Makanaka glacial deposits (after Porter, 1979c; Wolfe *et al.*, 1997) and ^{36}Cl sample sites. Younger Makanaka deposits are lightly shaded; Older Makanaka deposits are darkly shaded; sampled outwash channel and outwash fan on south flank are outlined in black. Key for sampling sites: BF, boulder fan; Mo, Older Makanaka moraine; My, Younger Makanaka moraine; OC, outwash channel; IB, incised bedrock. Individual boulders within each of our sampling groups are indicated on the insets at the bottom of the figure

subdued and not easily traceable on the landscape. We therefore sampled boulders toward the distal end of the moraines that were located in areas that were relatively flat to minimise the possibility of boulder movement after deposition. We restricted sampling to large (usually at least 1 m in diameter) boulders that projected above the surrounding matrix to minimise potential effects of episodic shielding by snow, volcanic ash or aeolian material on cosmogenic nuclide production, as well as from leakage of low-energy neutrons from the sides of the boulders (Zreda *et al.*, 1993; Masarik and Wieler, 2003). Significant quantities of ash or aeolian sediment were not observed in the crevices of any of the landforms, which suggests that the sampled boulders have probably been exposed to cosmic rays continuously since the landforms stabilised. Furthermore, sampling surfaces with evidence of ventifaction, spalling and other visible signs of erosion were avoided.

Laboratory methods

We measured the thickness of each sample to calculate the depth-integrated production rate. Samples were then crushed and sieved to isolate the 0.25–1.0 mm size fraction, which was treated with 3% HNO_3 overnight and rinsed in deionised water to remove atmospheric ^{36}Cl. Chlorine was liberated from the silicate matrix using both open vessels (loosely capped Teflon bottles) and closed vessels (high-pressure acid-digestion bombs). The use of open vessels has been the standard method

DOI: 10.1002/jqs

for extracting ^{36}Cl (Zreda, 1994), but the recent development of the closed-vessel technique combined with the use of a ^{35}Cl-enriched isotopic 'spike' (Desilets *et al.*, 2006) offers several advantages, including smaller sample sizes and more precise total chlorine determinations. Experimental data indicate that reproducible results can be obtained from both extraction methods (Desilets *et al.*, 2006). We did not observe any trends or biases in the Makanaka ^{36}Cl ages determined by either method.

Chlorine was precipitated as AgCl, purified of sulphur (^{36}S is an isobar of ^{36}Cl and interferes with the measurement of ^{36}Cl), and the ^{36}Cl/Cl was measured using accelerator mass spectrometry (AMS) at PRIME Lab, Purdue University. Total Cl was determined using the ion-specific electrode method (Aruscavage and Campbell, 1983) at MZ's laboratory at the University of Arizona. For open vessel samples, total Cl measurements were repeated a minimum of three times until the standard error of the mean fell below 5% of the total chlorine concentration. For closed-vessel samples, only one measurement of total Cl was required, and a precise determination of the total Cl was made from measurement of ^{37}Cl/^{35}Cl on spiked samples just after the AMS measurement of ^{36}Cl/Cl.

Major and trace elements that have high thermal neutron cross-sections (B, Sm and Gd, among others) compete with ^{35}Cl for thermal neutrons and must therefore be taken into account when calculating the cosmogenic production rate. Major elements were measured using inductively coupled plasma optical emission spectroscopy, selected trace elements with inductively coupled plasma mass spectrometry, and boron was measured using prompt gamma ray activation analysis, all at Activation Laboratories, Inc., Ontario, Canada (analytical data are provided in the Appendix, Table A.1). U and Th were measured using instrumental neutron activation analysis, also at Activation Laboratories. U and Th are important because neutrons produced from radioactive decay of these elements produce ^{36}Cl by activation of ^{35}Cl. This nucleogenic component must be subtracted from the total measured ^{36}Cl to obtain the cosmogenic ^{36}Cl that is used for the age calculation. The magnitude of the nucleogenic component in our samples ranged from 0.1% to 3.0% of the total measured ^{36}Cl inventory.

Cosmogenic ^{36}Cl production rates

Cosmogenic ^{36}Cl surface exposure ages were calculated using a new approach that is being implemented in the ACE (formerly iCRONUS) cosmogenic dating software (Anderson *et al.*, 2007) using the following production rates: 71.6 ± 3.8 atoms ^{36}Cl $(\text{g Ca})^{-1}\ \text{a}^{-1}$, 155.1 ± 9.6 atoms ^{36}Cl $(\text{g K})^{-1}\ \text{a}^{-1}$ and 676 ± 40 fast neutrons $(\text{g air})^{-1}\ \text{a}^{-1}$. A detailed discussion of the cosmogenic ^{36}Cl production rates used in this study is included in Appendix A.

Landform ages and propagation of uncertainties

Calculating landform ages based on a population of cosmogenic ^{36}Cl surface-exposure ages can be done either by taking the weighted mean of the individual samples or by assuming the oldest age does not contain an inherited cosmogenic component and therefore best approximates the true age of the landform. We prefer the former because it does not place undue weight on a single sample. Our conclusions below, however, would not change significantly if we used the oldest sample from either deposit, rather than the weighted mean of the sample ages, to approximate the landform age.

Landform ages are reported as the weighted mean (μ') of the individual sample ages using $1/\sigma_i^2$ weighting, where σ_i is the error associated with the individual sample measurement (Bevington and Robinson, 1992, equation 4.17). The σ_i values used in the landform age calculation include the analytical (or random) uncertainties. Analytical uncertainties associated with the ^{36}Cl/Cl and Cl measurements for the individual samples were calculated using the square rule for variance propagation. The uncertainty associated with muogenic production is negligible for our samples because muon production accounts for only a few per cent of the total production at altitudes of >3000 m. The nucleogenic component of ^{36}Cl can be calculated to within ~10–20% (F. M. Phillips, pers. comm., New Mexico Tech, 2001) and, given the small magnitude of the nucleogenic component in our samples, the uncertainty associated with this correction is also negligible compared to the total analytical error.

Uncertainties were combined using the usual square rule for combining variances and propagated using the law of combination of errors, neglecting covariance terms (Bevington and Robinson, 1992, equation 3.13). We calculated both the standard error of the weighted mean (Bevington and Robinson, 1992, equation 4.19) and the weighted average variance of the data (Bevington and Robinson, 1992, equation 4.22), and took the square root of the larger of the standard error and weighted average variance as the uncertainty of the calculated landform age (i.e. weighted average standard deviation), which we report at the 95% confidence level (2σ). For clarity, the landform age $T \pm t\,(n = 5)$ means that the weighted mean age T of five boulder ages should be within $\pm\, t$ of the weighted mean age of any other five boulder ages from the same surface, 95% of the time.

Ice mass balance modelling

We used a positive degree day (PDD) model of glacier mass balance to determine the climatic conditions during the Makanaka glaciations (Braithewaite, 1995). Our model uses surface temperature and snow accumulation to calculate ice mass balance and equilibrium line altitude (ELA), from which ice extent can be inferred. The required inputs included: (1) the surface topography of Mauna Kea, for which a 10 m resolution digital elevation model from the United States Geological Survey was used (www.soest.hawaii.edu/coasts/data/hawaii/dem.html, accessed in December 2005); (2) the spatial distribution of long-term mean monthly precipitation based on 1971–2000 normals developed by the PRISM group at Oregon State University, http://www.prism.oregonstate.edu/products/pacisl.phtml, and the Natural Resources Conservation Service (NRCS) Water and Climate Center, ftp://ftp.ftw.nrcs.usda.gov/pub/ams/prism/data/states/hi/hi_rast_meta.html, accessed in December 2005); (3) monthly temperatures at Mauna Loa Observatory (19.53° N, 155.58° W, 3395 m a.s.l.) and Hilo (19.72° N, 155.07° W, 10 m a.s.l.) (Western Regional Climate Center of the Desert Research Institute; http://www.wrcc.dri.edu, accessed in January 2006); and (4) lapse rates calculated using linear regression of 00UTC monthly radiosonde mandatory pressure-level reported temperatures (Integrated Global Radiosonde Archive, Durre *et al.*, 2006) between sea level and 5000 m a.s.l. over the period 1957–2005. Degree day factors of 3 (snow) and 8 (ice) mm $\text{d}^{-1}\ ^{\circ}\text{C}^{-1}$ (water equivalent) are assumed in the PDD model, as is a standard deviation of 2.8°C for the monthly mean surface

DOI: 10.1002/jqs

temperature, which is based on the Hilo weather station data. A 0°C cut-off is assumed to calculate the fraction of total precipitation over Mauna Kea falling as snow; below 0°C all precipitation is assumed to fall as snow; above 0°C as rain. The total amount of snow accumulation over a year is determined using observed monthly precipitation rates and temperatures that are generated from monthly sea-level temperature (SLT) at Hilo and interpolated to high elevations using radiosonde-inferred lapse rates. Yearly ablation is calculated by determining the spatial distribution of PDDs over the region and using the degree day factors for snow and ice. Finally, glacier mass balance is calculated as snow accumulation minus ablation, and the ELA is defined as the elevation at which the computed mass balance is zero.

Cosmogenic ^{36}Cl exposure ages

We determined surface-exposure ages of nine boulders collected from the Makanaka moraines: three from the Older Makanaka moraine on the north-west flank of the volcano, three from the nearby Younger Makanaka moraine, and three from the Younger Makanaka moraine on the south-west flank of the mountain. We also determined surface-exposure ages of two boulders from an outwash channel and eight boulders from an outwash fan located just below a prominent lobe of the Makanaka moraine on the south flank of the volcano. In addition, one bedrock surface at the bottom of a gully incised deeply into a lava flow by running water was dated.

Glacial landforms (moraines)

Older Makanaka moraine

In the area in which we sampled, the Older Makanaka moraine (Fig. 1, Mo) has a broad, flat top, and contains numerous small (mostly <1 m) boulders and cobbles, some of which are deeply rooted in the matrix. Hawaiites derived from the nearby lava flows of the Laupahoehoe Group dominate; basalts of the Hamakua Group are rare. Exposure ages of three boulders from the Older Makanaka moraine range from 21.6 ± 2.9 ka (the uncertainties are 2σ, unless stated otherwise) to 25.2 ± 2.5 ka (Fig. 2 and Table 1), and have a weighted mean of 23.1 ± 2.5 ka. This age will be used in further discussion.

Younger Makanaka moraine

The Younger Makanaka moraine forms a nearly continuous annulus around the summit of Mauna Kea (Fig. 1, My). It overlies the Older Makanaka till in some places, and hawaiitic lava flows of the Laupahoehoe Group elsewhere (hence the dominant lithology is hawaiite). Six sampled boulders – three in

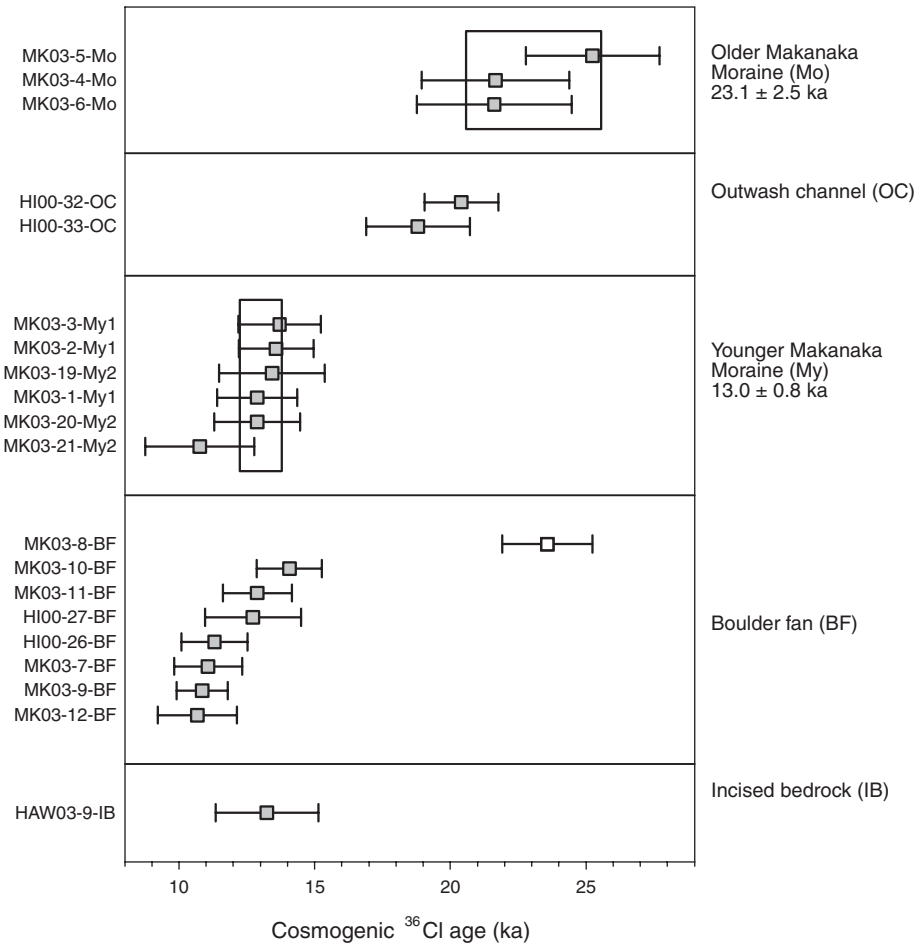

Figure 2 Cosmogenic ^{36}Cl ages for the Makanaka surfaces. The open square denotes an outlier not used in the calculation of surface ages (see text for discussion). Error bars are $\pm 2\sigma$. Boxes represent the weighted mean age of the landform plus and minus the larger of the two errors, weighted standard deviation and weighted error of the mean, respectively, reported as 2σ

DOI: 10.1002/jqs

Table 1 ^{36}Cl results for Mauna Kea landforms

Sample ID	Latitude (°N)	Longitude (°W)	Elevation (m)	Thickness (g cm^{-2})	$P_{36,eff}$[a] (N_{36} g^{-1} a^{-1})	$N_{36,cosmog}$[b] (Ma_{36} g^{-1})	^{36}Cl age[c] (ka)	Δ age (%) due to erosion[d]			Δ age (%)[e] No sea-level
								1 mm ka^{-1}	2 mm ka^{-1}	3 mm ka^{-1}	
Older Makanaka moraine											
MK03-5-Mo	19.851	155.497	3623	8.4	78.3	1.920	25.2 ± 2.5	−4.8	−8.1	−10.4	1.4
MK03-4-Mo	19.851	155.498	3618	5.6	66.6	1.407	21.7 ± 2.7	−2.6	−4.5	−5.8	1.3
MK03-6-Mo	19.853	155.496	3626	5.6	59.1	1.247	21.6 ± 2.9	−1.1	−2.0	−2.8	1.3
Weighted mean age of landform							23.1 ± 2.5				
Outwash channel											
HI00-32-OC	19.774	155.471	3227	10.8	49.5	0.988	20.4 ± 1.4	−2.2	−3.7	−4.9	1.2
HI00-33-OC	19.774	155.471	3227	16.2	39.9	0.735	18.8 ± 1.9	−0.2	−0.3	−0.1	1.1
Younger Makanaka moraine											
MK03-3-My1	19.841	155.504	3601	8.4	56.4	0.761	13.7 ± 1.5	−1.5	−2.8	−3.8	−0.1
MK03-2-My1	19.844	155.501	3607	5.6	52.1	0.697	13.6 ± 1.4	−0.3	−0.5	−0.6	−0.4
MK03-19-My2	19.813	155.512	3633	7.0	71.3	0.943	13.4 ± 1.9	−2.4	−4.3	−6.0	−0.3
MK03-20-My2	19.813	155.512	3634	7.0	51.1	0.649	12.9 ± 1.6	−0.5	−1.0	−1.3	−0.2
MK03-1-My1	19.844	155.501	3615	5.6	45.4	0.577	12.9 ± 1.5	−0.3	−0.5	−0.6	−0.2
MK03-21-My2	19.813	155.512	3635	7.0	56.5	0.601	10.8 ± 2.0	−1.3	−2.3	−3.3	−0.8
Weighted mean age of landform							13.0 ± 0.8				
Boulder fan											
MK03-8-BF[f]	19.788	155.451	3531	7.0	51.5	1.182	23.6 ± 1.7	0.2	0.6	1.3	1.0
MK03-10-BF	19.788	155.449	3516	5.6	58.1	0.804	14.1 ± 1.2	−1.8	−3.3	−4.6	−0.2
MK03-11-BF	19.788	155.449	3514	8.4	50.1	0.636	12.9 ± 1.3	−1.1	−2.1	−2.9	−0.3
HI00-27-BF	19.790	155.452	3475	8.0	52.2	0.655	12.7 ± 1.8	−1.5	−2.8	−3.9	−0.3
HI00-26-BF	19.790	155.452	3475	10.6	45.5	0.508	11.3 ± 1.2	−0.9	−1.7	−2.3	−0.6
MK03-7-BF	19.788	155.451	3527	5.6	47.1	0.515	11.1 ± 1.3	−0.7	−1.3	−1.8	−0.7
MK03-9-BF	19.788	155.449	3516	7.0	46.4	0.498	10.9 ± 0.9	−0.7	−1.2	−1.7	−0.7
MK03-12-BF	19.788	155.449	3518	4.2	61.8	0.652	10.7 ± 1.5	−1.7	−3.2	−4.5	−1.0
Incised bedrock											
HAW03-9-IB	19.776	155.560	2035	8.0	18.2	0.238	13.2 ± 1.9	−0.3	−0.6	−0.9	−0.5

A topographic shielding correction factor of 0.998–1.000 was included in the calculations for all samples except HAW03-9-IB (0.912).
[a] Effective (average) production rate for the exposure duration.
[b] Inventory of cosmogenic ^{36}Cl, in millions of atoms (Ma) per gram of rock.
[c] Uncertainties in sample and landform ages are reported at the 2σ (95%) confidence level.
[d] Percentage difference in age if erosion (at rates shown) is taken into account (negative numbers denote younger age).
[e] Percentage difference in age if production rates are not corrected for eustatic sea-level changes (negative numbers denote younger age).
[f] Exposure age is >2σ from the weighted mean. Not included in the final calculation of the landform exposure age.

DOI: 10.1002/jqs

the north-west (My1) and three in the west (My2) – have exposure ages ranging from 10.8 ± 2.0 ka to 13.7 ± 1.5 ka, and a weighted mean of 13.0 ± 0.8 ka. This age will be used in further discussion.

Glaciofluvial landforms

Outwash channel

A glaciofluvial outwash channel located on the south flank of the volcano is littered with well-rounded boulders up to 1 m in diameter (Fig. 1, OC). The material originated in the belt of Makanaka moraines that exists just above the outwash. Two boulders from the outwash channel have ages of 20.4 ± 1.4 ka and 18.8 ± 1.9 ka, indicating the formation of the outwash deposit during and possibly shortly after the Older Makanaka glacial episode.

Boulder fan

A fan located on the south flank of the volcano contains numerous boulders that were excavated from the Younger Makanaka moraine and transported a few hundred metres downslope (Fig. 1, BF). Exposure ages of the boulder fan range from 10.7 ± 1.5 ka to 14.1 ± 1.2 ka, excluding sample MK03-8-BF, which clearly contains a significant inherited ^{36}Cl component. The exposure age of this sample (23.6 ± 1.7 ka) is nearly twice that of each of the other seven boulders from the same landform, and its chemical composition indicates that it originated from the Hamakua Volcanic Group, an older stratigraphic unit on Mauna Kea (Table A.1). We considered this sample an outlier and removed it from further discussion. The timing and position of the fan just below the Makanaka moraine suggest that it likely formed during or shortly after the Younger Makanaka glaciation.

Incised bedrock

Far below the Makanaka moraines and outwash/fan deposits, running water produced deep incisions in bedrock surfaces. Today, these incisions are dry most of the time because of the aridity of the area and the high permeability of the volcanic rocks. We sampled one area of incised bedrock present on the southwest side of the mountain, at an elevation of 2035 m a.s.l. (Fig. 1, IB). The incision is 7 m deep, enough to remove most of the existing cosmogenic inventory and reset the cosmogenic clock. A flat surface at the bottom of the incision yielded an exposure age of 13.2 ± 1.9 ka, lending further support for glaciofluvial activity during Younger Makanaka time.

Geological considerations

Geological factors that may affect the cosmogenic nuclide inventory of a sample include inheritance, episodic shielding, boulder erosion, post-depositional boulder movement and deflation of the landform surface (i.e., exhumation of previously buried surface). Inherited ^{36}Cl atoms can accumulate in boulders before or during glacial transport, which results in exposure ages that are older than the true age of the landform (Dzierzek and Zreda, 2007). Inheritance does not appear to be a significant problem in our samples, with the exception of sample MK03-8-BF (Fig. 2), as stated above. Inheritance of a lesser magnitude (e.g. <10% of the landform age) cannot be quantitatively addressed because of uncertainties in the production rates and the potential effects of episodic shielding and erosion.

Boulder surfaces can be episodically shielded by volcanic ash, wind-blown sediment or snow. Cover by ash and/or sediment partially shields the boulder surface from cosmic rays and, therefore, actual production rates would be lower than calculated rates. We did not observe any evidence of ash or aeolian sediment in the crevices or between boulders on the glacial landforms. Low-energy (thermal and epithermal) neutrons interact with water (as snow), which, in contrast to ash and sediment, can either increase or decrease ^{36}Cl production at the rock surface, depending on the thickness of snow. While snow cover can potentially be a significant source of error in high-altitude environments in the tropics, snow and ice in the summit area of Mauna Kea quickly sublimate after precipitation events, rarely lasting more than a few days at the ground surface.

The impact of postglacial surface erosion on ^{36}Cl exposure ages depends on the contribution of production by neutron activation to the total production rate, and consequently on the concentrations of Cl, K and Ca in the samples. We calculated ^{36}Cl exposure ages for each boulder using surface erosion rates of 0, 1, 2 and 3 mm ka^{-1}. Our calculations indicate that erosion of boulder tops would change the exposure ages by an average of <3% (Table 1) and, therefore, we calculated the landform ages using the zero erosion scenario.

The effect of post-depositional movement of boulders on ^{36}Cl exposure ages depends on the size of the boulders sampled and when they moved. For boulders that are >1 m in diameter, such as those sampled in this study, movement results in exposure of a 'new' boulder top that was previously shielded (or partially shielded) from cosmic rays. If movement occurred immediately after deposition, then the new boulder top would be exposed to cosmic rays at essentially the same time as it was deposited and the boulder would yield a reliable exposure age. If, however, it rolled several thousand years after initial deposition, then it would yield an exposure age that is far too young. The magnitude of the offset depends on when and how it rolled and where the new boulder top was prior to movement. If several boulders are sampled and all have rolled at some time following initial deposition, then the spread of boulder ages would be large. We attempted to avoid this problem by sampling boulders in areas that were locally flat, thus reducing the chance of post-depositional movement. The tight clustering of ages for the Makanaka moraines (Table 1) indicates that this strategy was largely successful.

Finally, the impact of landform deflation on our ^{36}Cl ages should be minimal because it requires substantial lowering (at least 2–3 m) of the original surface. Eroded landforms exhibit a wide range of ages, with the oldest boulder age being closest to the true landform age (Hallet and Putkonen, 1994; Zreda *et al.*, 1994). The tight clustering of ages for the Makanaka moraines (Table 1) indicates that significant landform deflation has not occurred.

Interpretation of landform ages

Based on the ^{36}Cl results and stratigraphic relationships of the glacial and glaciofluvial landforms, we conclude that the outwash channel was formed by waters from melting of the

DOI: 10.1002/jqs

Older Makanaka ice cap, whereas both the fan and incised bedrock were formed by meltwater from the Younger Makanaka ice cap. As the ice caps receded, glacial meltwater cut through and washed out the moraines in a few places, redepositing clastic material downstream in channels and fans. The same meltwater also created the bedrock incisions further downgradient. If this scenario is correct, then exposure ages from the glaciofluvial landforms should be viewed as auxiliary secondary evidence that support the moraine ages, which we consider to be our primary evidence for the timing of deglaciation. We have not assigned an age for any of the three glaciofluvial landforms, as we did for the moraines, because these landforms were likely formed over some (unknown) period of time as the glaciers receded. Thus, they represent processes rather than datable events. However, the similarity between the mean ages of the moraines and the earliest evidence of glaciofluvial activity does suggest a common genesis for the landforms.

It is possible that the difference between the oldest and the youngest ages corresponds to the duration of the glaciofluvial activity for the Younger Makanaka glaciation; i.e., the oldest sample (MK03-10-BF, 14.1 ka) corresponds closely to the peak of glaciation while the youngest sample (MK03-12-BF, 10.7 ka) reflects the end of fluvial activity. However, it is also possible that clastic material in the boulder fan was unstable after initial deposition, and that the spread of boulder ages is due to a combination of original exposure followed by boulder movement and possibly limited fluvial transport and redeposition. Our data do not allow us to differentiate between these scenarios.

Climatic inferences from Makanaka ice caps

A comparison (Fig. 3) of our glacial chronology with the pollen-based record of temperature and precipitation from O'ahu (Hotchkiss and Juvik, 1999) and the alkenone-based SST record from the subtropical North Pacific (Lee and Slowey, 1999; Lee *et al.*, 2001), shows that the two Makanaka glaciations were associated with large changes of temperature or precipitation (but not necessarily both!). At sea level, assuming our ^{36}Cl ages are accurate, the Older Makanaka climate was colder than today by ~3°C and as wet as today. In contrast, the Younger Makanaka climate was nearly as warm as today, but significantly wetter. This suggests that expansion of the Older Makanaka ice cap was caused largely by a decrease in temperature, whereas increased precipitation drove the Younger Makanaka glaciation. However, because the alkenone and pollen sites are at and near sea level (463 m a.s.l.), respectively, and the glacial sites are near the top of Mauna Kea (~3600 m a.s.l.), this conclusion is only qualitative and provisional. In the following sections, we examine this provision and draw quantitative conclusions about glacial-time climates on the upper reaches of Mauna Kea.

One approach to reconstructing palaeoclimate is to estimate palaeo-ELAs (p-ELAs), calculate their depression with respect to the modern ELA and infer the corresponding changes of temperature and/or precipitation rate. At least one additional palaeoclimatic record is necessary for a unique solution because ELA depends on both temperature and precipitation. We used two: a pollen-derived temperature record from a low-elevation (463 m) site on O'ahu (Hotchkiss and Juvik, 1999) and an alkenone-based SST record from the subtropical North Pacific (Lee and Slowey, 1999; Lee *et al.*, 2001). During our analysis, it was necessary to transfer these low-elevation temperatures to the elevation of the Makanaka moraines. This transfer encompasses more than 3000 m of altitude, and therefore presents a potential problem because of an apparent inconsistency between palaeotemperature reconstructions at sea level and at high altitudes elsewhere in the tropics. For example, Last Glacial Maximum (LGM) reductions in tropical Pacific SSTs based on marine proxy data are of the order of 2–3°C (Lee and Slowey, 1999; Lea *et al.*, 2000), whereas tropical glacier ELA depressions of approximately 1000 m imply twice as large cooling at higher elevations (Crowley, 2000; Mark

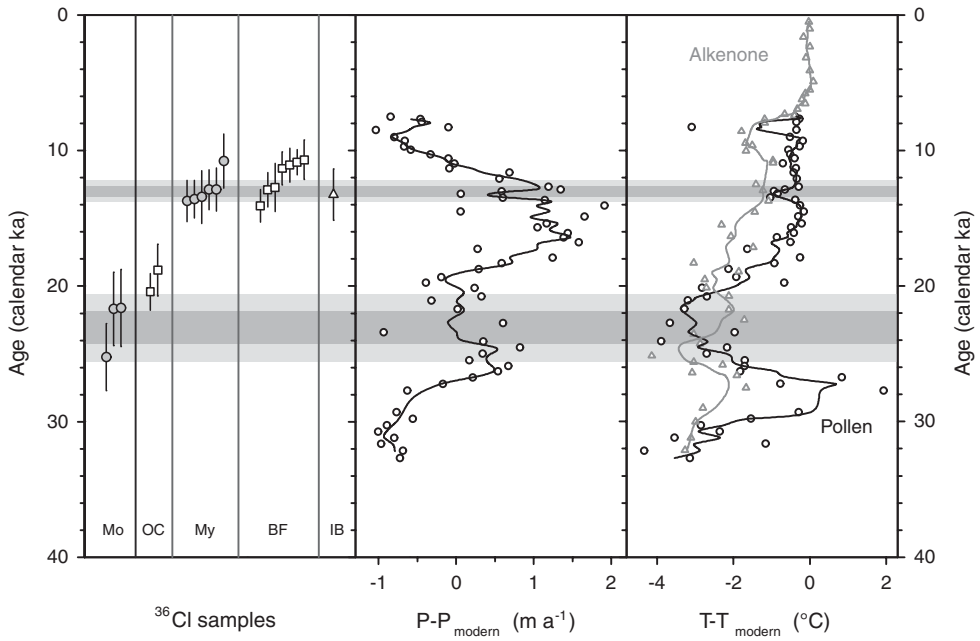

Figure 3 Makanaka glacial ages for individual samples (left panel), precipitation reconstructions from the pollen record of Hotchkiss and Juvik (1999) (centre panel), and temperature reconstructions from the pollen (Hotchkiss and Juvik, 1999) and alkenone (Lee and Slowey, 1999; Lee *et al.*, 2001) records (right panel). Solid lines are three-point moving averages. Horizontal bands denote ^{36}Cl ages of moraines, 1σ limits (darkly shaded), and 2σ limits (lightly shaded)

DOI: 10.1002/jqs

et al., 2005). Falling between these extremes, modelling by Hostetler and Clark (2000) suggests that an LGM glaciation on Mauna Kea required at least a 3.5°C cooling at the ELA based on modern lapse rates.

Evidence reviewed by Farrera *et al.* (1999) suggests that steeper (more negative) lapse rates during the LGM, particularly in the Pacific Ocean region, could reconcile differences between low- and high-altitude palaeotemperature reconstructions. Here we examine this possibility for Mauna Kea using glacier mass balance modelling in concert with our cosmogenic ^{36}Cl glacial chronology. Past climate conditions, specifically high-elevation annual temperatures and precipitation rates, are reconstructed for the Younger and Older Makanaka glaciations and compared with the modern climate. A mechanism is then proposed through which glacial-time lapse rates could be steeper than those today, allowing for steeper lapse rates in the tropical Pacific during the Late Pleistocene (Farrera *et al.*, 1999) that could reconcile modest cooling at sea level and greater cooling at mountain altitudes.

Geological proxy records of palaeoclimate

Our glacier mass balance model uses geological information of three types as input: (1) ages of moraines; (2) extents of moraines; and (3) independent proxy records of temperature. The cosmogenic ^{36}Cl chronology of the terminal moraines places glacial events on an absolute timescale, permitting comparisons with other palaeoclimatic proxy data. The extents of the former ice caps, which are extracted from elevations of the terminal moraines, contain information on the magnitude of glacial-time climate change. Finally, for independent estimates of temperature, we used two records in an effort to avoid placing too much emphasis on a single proxy record: (1) the O'ahu pollen-derived temperature record, which was used to calculate SLTs near Hawai'i during Makanaka glacial times; and (2) the alkenone-based SST record from the subtropical North Pacific. The O'ahu pollen record spans ca. 30 to 8 ka, whereas the alkenone SST record spans approximately the last 30 ka. Both of these time intervals include the two Makanaka glaciations.

Timing of Makanaka ice caps (from ^{36}Cl dating)

The mean ^{36}Cl exposure ages for the Younger and Older Makanaka moraines are 13.0 ± 0.8 ka and 23.1 ± 2.5 ka, respectively (Table 1).

Geometry of Makanaka ice caps (from moraine locations)

The extent of the Younger Makanaka ice cap was reconstructed from the distribution of the terminal moraines as mapped by Porter (1979c) and Wolfe *et al.* (1997), and includes only the parts of the terminus not obstructed by volcanic deposits. The average elevation of the maximum extent of the Younger Makanaka ice cap is 3500 ± 50 m a.s.l. (1σ) using Porter (1979c) and 3490 ± 80 m a.s.l. using Wolfe *et al.* (1997). However, terminal moraines are present up to 3610 ± 60 m a.s.l. Landforms other than moraines dominate the landscape above this elevation. This belt of terminal moraines indicates that the elevation of the ice cap margin fluctuated by ~110 m, which is not unexpected based on observations of the response of modern glaciers to short-term climatic fluctuations (Oerlemans, 2001). After correction for isostatic sinking of the island at the rate of 2.5 ± 0.5 m ka^{-1} (Porter, 1979a), the average elevation of the Younger Makanaka moraines during glacial times was 3590 ± 80 m a.s.l.

Older Makanaka moraines are exposed on the north-west and east flanks of Mauna Kea, as well as several small areas on the north and south flanks just below the Younger Makanaka margin (Fig. 1). The extent of the Older Makanaka moraine slightly beyond the Younger Makanaka limit at several locations and inside the Younger Makanaka elsewhere suggests that the two ice margins were not very different; hence we use the same range of 3500 ± 50 m a.s.l. to 3610 ± 60 m a.s.l. for the older moraine. Corrected for subsidence, the average elevation of the Older Makanaka ice cap was 3610 ± 80 m a.s.l.

Near-sea-level temperature changes

The O'ahu pollen record was constructed using multiple botanical species to create a pollen abundance index, which was then compared to modern climate and historical vegetation records to infer past temperature and precipitation conditions (Hotchkiss and Juvik, 1999). Temperature is more useful for our purposes because we can transfer temperature from one altitude to another using lapse rates, whereas precipitation rates cannot be transferred directly because of several complicating factors, including multiple moisture sources and variable orographic effects. SSTs in the tropical North Pacific were inferred from alkenones in marine sediments from two piston cores – PC17 and PC20 – located off Kahe Point on the southwestern shore of O'ahu (Lee and Slowey, 1999; Lee *et al.*, 2001).

Near-sea-level temperatures during Makanaka times were estimated using the pollen-based air temperature and alkenone-based SST records (Fig. 3; Table 2) averaged over the appropriate time for the two glaciations. We took the proxy data and the chronologies, as well as our own ^{36}Cl glacial chronology, at face value; that is, we did not force the coolest temperatures reconstructed in the proxy records to coincide with the ^{36}Cl ages of the Older Makanaka glaciation (or vice versa). Although there are some small differences between the two records, we note three things: (1) the overall warming trend between ca. 30 and 10 ka is essentially the same in both records; (2) cooling during the Older Makanaka glaciation in the alkenone record (2.55 ± 0.43°C; 1σ) is nearly identical to that in the O'ahu pollen record (2.93 ± 0.40°C); and (3) cooling during the Younger Makanaka glaciation was similar between the two records: 1.23 ± 0.03°C in the alkenone record and 0.66 ± 0.19°C in the pollen record. While we prefer the land-based pollen record, which reflects air temperature directly, to the alkenone record, which reflects SSTs, our conclusions would not change significantly regardless of which record we used. But we do have to assume that the temperature changes in and near O'ahu that are inferred from these records are the same as temperature changes at low elevations on the island of Hawai'i, some 300 km to the east/south-east.

Modelling of glacier mass balance

Our model initially calculates the permissible parameter space using mean SLT, the modern annual precipitation rate at an elevation of 3800 m a.s.l. (close to the Makanaka-time snowlines), and a range of moraine elevations. First, we show

DOI: 10.1002/jqs

Table 2 Summary of modelling results

Time	Age (ka)	Ice margin (m)	ELA (m)	$E_{0\ July}$ (m)	$E_{0\ annual}$ (m)	Lapse rate (°C km^{-1})	$\Delta T_{463\ m}$ (°C)	$T_{0\ m}$ (°C)	$T_{3800\ m}$ (°C)	T_{ELA} (°C)	$T_{ELA\ July}$ (°C)	$P_{3800\ m}$ (mm a^{-1})
Modern	0	None	4680 ± 50	4690	4470	−4.97	0	22.3	3.43	−0.94 ± 0.25	0.18 ± 0.10	450
Pollen												
Younger Makanaka	13.0 ± 0.8	3590 ± 80	3780 ± 20	3955	3775	−5.71	−0.66 ± 0.19	21.64	−0.06	0.06 ± 0.19	0.92 ± 0.05	1970 ± 120
Older Makanaka	23.1 ± 2.5	3610 ± 80	3805 ± 20	3840	3650	−5.29	−2.93 ± 0.40	19.37	−0.73	−0.76 ± 0.40	0.29 ± 0.07	1100 ± 130
Alkenone												
Younger Makanaka	13.0 ± 0.8	3590 ± 80	3785 ± 20	3930	3750	−5.60	−1.23 ± 0.03	21.07	−0.21	−0.13 ± 0.03	0.80 ± 0.05	1735 ± 95
Older Makanaka	23.1 ± 2.5	3610 ± 80	3800 ± 20	3860	3675	−5.36	−2.55 ± 0.43	19.75	−0.62	−0.62 ± 0.43	0.34 ± 0.07	1230 ± 145

Abbreviations for model parameters:

- ELA = equilibrium line altitude.
- $E_{0\ July}$ = July 0°C isotherm.
- $E_{0\ annual}$ = annual 0°C isotherm.
- $\Delta T_{463\ m}$ = difference in temperature between glacial periods and today at 463 m a.s.l.
- $T_{0\ m}$ = air temperature at sea level.
- $T_{3800\ m}$ = air temperature at 3800 m a.s.l.
- T_{ELA} = annual air temperature at ELA.
- $T_{ELA\ July}$ = July air temperature at ELA.
- $P_{3800\ m}$ = annual precipitation at 3800 m a.s.l.

that no reasonable amount of precipitation can produce glaciers of the size consistent with the Makanaka moraines using modern fixed lapse rates. Next, we show that temperature lapse rates on Hawai'i are a function of precipitation, and demonstrate that increased precipitation and correspondingly steeper lapse rates during glacial times could produce ice caps that are consistent with the moraine distribution. Finally, we quantitatively reconstruct high-elevation temperature and precipitation during glacial times and speculate on the origin of moisture that caused precipitation sufficient to grow and maintain ice caps on Mauna Kea.

Establishing model parameter space

To infer first-order climate differences from present conditions, we reduced glacial SLTs by a uniform amount and increased precipitation over the volcano, also by a uniform amount. (We also tried increasing precipitation by a uniform factor rather than a uniform amount, but the resulting ice cap was unreasonably asymmetric and the calculated precipitation at sea level was unreasonably high. Thus, we do not discuss this case here.) Ice extent elevations were determined assuming that at steady state the area-integrated mass balance over the total ice sheet area is zero. This assumption ignores spatial variability in the elevation of ice extent over the volcano, but is reasonable given the uncertainties in the elevation of moraines. Modelled ELAs were also computed from the mass balance model, but are not directly comparable with the moraine data and therefore are not used here.

Assuming a modern precipitation regime (450 mm a^{-1} at 3800 m a.s.l.), a minimum 4°C reduction in SLT is required to produce any glaciers, and cooling by 6°C is required to produce glaciers that descend to the lower altitude of the Makanaka moraines (~3600 m a.s.l.) (Fig. 4(a)). Although this result is compatible with an 800–900 m reduction in ELA on Mauna Kea (Porter, 1979a; Hostetler and Clark, 2000), it is inconsistent with SST changes for the LGM tropical Pacific of only 2–3°C (Lee and Slowey, 1999). It falls between other modelled estimates of 3.5°C (Hostetler and Clark, 2000) and 6–7°C (Blard *et al.*, 2007), which were calculated assuming a precipitation rate near the summit of 1600 mm a^{-1} and 300 mm a^{-1}, respectively. In contrast, assuming a modern temperature regime (SLT of 22.3°C), no amount of increased precipitation will result in the glaciation of Mauna Kea (Fig. 4(a)). Yet based on the O'ahu pollen record (Fig. 3), the Younger Makanaka glaciation occurred under essentially modern air temperatures and precipitation rates near sea level that were only ~1 m a^{-1} higher than today.

To account for these discrepancies, we postulate that precipitation may play an even stronger role than previously assumed. There is evidence for steeper lapse rates in the tropical Pacific (Farrera *et al.*, 1999), and Crowley (2000) notes that with steeper lapse rates high elevations could become sufficiently cool to support glaciers. To examine this, we looked at seasonal differences in lapse rate at Hilo determined from radiosonde data, and found that they correlated with seasonal changes of precipitation at high altitude. Based on average monthly temperature and precipitation data, a linear relationship exists between precipitation and lapse rates at elevations between 0 and 5000 m a.s.l. ($R = -0.75$). On the basis of simple moist adiabatic lapse rate theory, this relationship would appear counterintuitive as a drier atmosphere implies steeper lapse rates. However, as the reconstructions infer that greater precipitation and colder summit temperatures were necessary for glaciation on Mauna Kea, assuming relatively minor

DOI: 10.1002/jqs

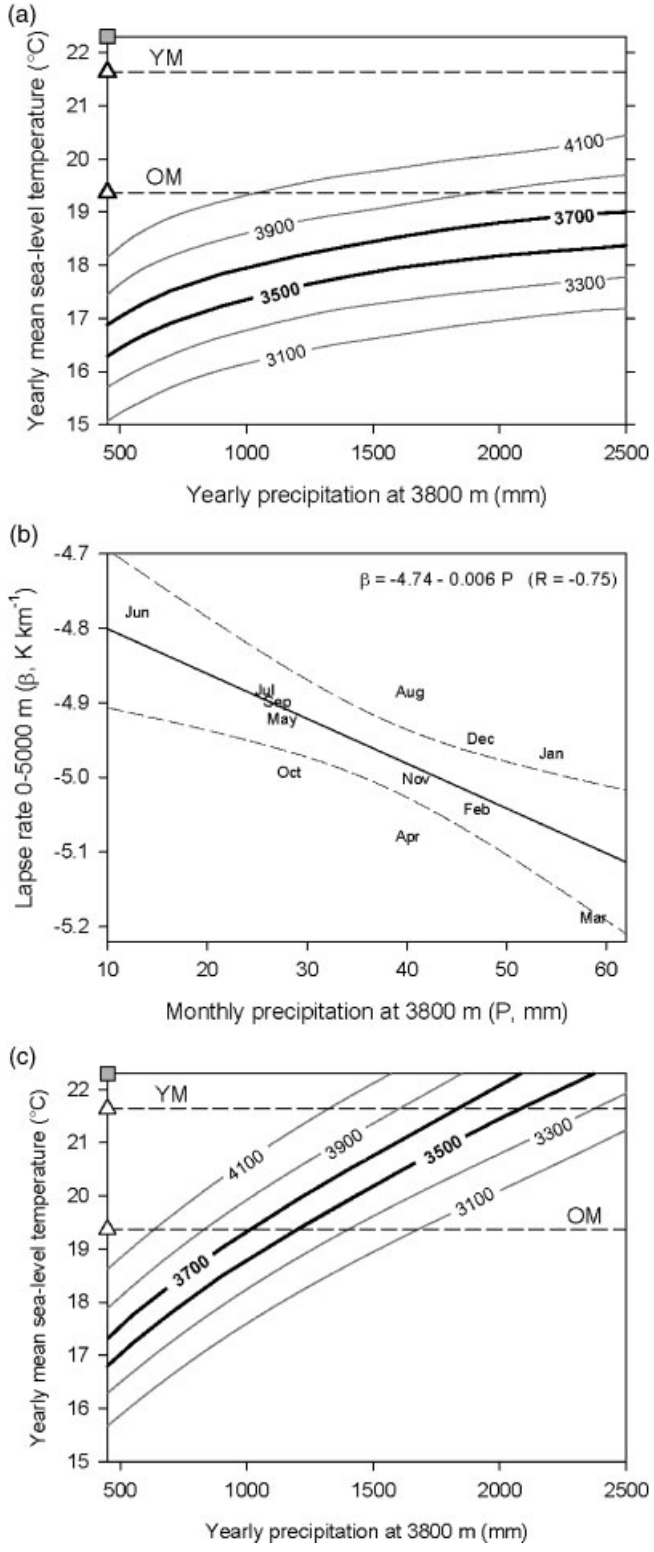

Figure 4 (a) Modelled ice extent elevation as a function of temperature and precipitation changes from those of today (22.3°C at sea level and 450 mm a^{-1} at 3800 m a.s.l., marked by the square in the top left corner). Thick lines at 3500 and 3700 m a.s.l. show the range of elevations of Makanaka moraines (see Fig. 1). Triangles and dashed lines show the pollen-derived temperatures for Younger Makanaka (upper line) and Older Makanaka (lower line) glaciations. (b) Observed changes in lapse rate between sea level and 5000 m a.s.l. (Integrated Global Radiosonde Archive; Durre *et al.*, 2006) as a function of mean monthly precipitation at 3800 m a.s.l. over Mauna Kea reported by the National Climate Data Center. (c) Modelled ice extent elevation as a function of temperature and precipitation changes from those of the present day when the variable lapse rate (Fig. 4(b)) is considered to be a function of precipitation

changes in SLT, a correlation between increased precipitation and steeper lapse rates is apparent. We therefore suggest that this correlation most likely reflects seasonal changes in the dominance of different weather regimes over Mauna Kea. Hostetler and Clark (2000) found that changes in the tropical inversion height over Hawai'i could produce colder conditions at mid-altitude and greater precipitation at high altitude. The correlation does not imply causality, but it does suggest a missing process in the mass balance model used to produce the results shown in Fig. 4(a). Farrera *et al.* (1999) suggest several different mechanisms to explain steeper LGM lapse rates in the tropical Pacific, including changes from an intensified hydrological cycle (Diaz and Graham, 1996). For Mauna Kea, there appears to be a seasonal signal embedded in the relationship as summer months generally have low precipitation and shallow lapse rates (less negative) while winter months generally have high precipitation and steeper lapse rates (Fig. 4(b)). On the basis of this correlation and the apparent glaciation of Mauna Kea during a period of increased precipitation, we assume a linear relationship between precipitation and lapse rates shown as the line of best fit in Fig. 4(b). This relationship suggests that a doubling of present-day precipitation would correspond to a steepening of the lapse rate of about 0.25°C km^{-1}.

Figure 4(c) shows the extent of glaciation as a function of temperature and precipitation departures from those of the present day when the relationship between lapse rate and precipitation shown in Fig. 4(b) is implemented into the mass balance model. Compared to Fig. 4(a), the ice extent is much more sensitive to precipitation changes. Without changing precipitation from that of the present day, a 5°C temperature depression is still required for glaciation. Conversely, if SLTs were held constant, glaciers consistent with the Makanaka moraines could be attained with precipitation of ~5 times that of today. If SLTs during Makanaka times were lower than today, as indicated by both the O'ahu pollen-based temperature record and the alkenone SST record, reasonable increases in precipitation, ranging from 2 to 4 times modern, could produce ice caps that are consistent with the Makanaka moraines.

In summary, our glacier mass balance model does not generate any ice on Mauna Kea using modern fixed lapse rates. But when lapse rates are adjusted for precipitation effects, the model produces ice caps consistent with the Makanaka moraines under reasonable climate regimes. Although the correlation of lapse rates with precipitation does not imply causality, it does explain the apparent discrepancy between SLTs and those at mountain altitudes, and allows glaciers to exist on Mauna Kea under the climatic conditions inferred from the independent climate proxy data.

Inferring Makanaka climates

Our glacier mass balance model permits quantitative estimates of climatic conditions on top of Mauna Kea during glacial times. The following modelling results were used in our analysis of palaeoclimatic variables: (1) spatial distribution of temperatures (July and annual) for the two Makanaka glacial times (Figs 5(a,b) and (d,e)); (2) spatial distribution of glacier net mass balance (Figs 5(c) and (f)) and the average ELA (Fig. 6); and (3) precipitation rate at 3800 m a.s.l. (Fig. 7). Table 2 summarises the climate modelling results.

A persistent feature of the spatial distribution of July and annual temperatures and of net mass balance is their radial near-symmetry (Fig. 5). (The small asymmetry is probably due to the slightly gentler and slightly cooler eastern slopes.) At 3800 m a.s.l., the Older Makanaka air was approximately 0.7°C

DOI: 10.1002/jqs

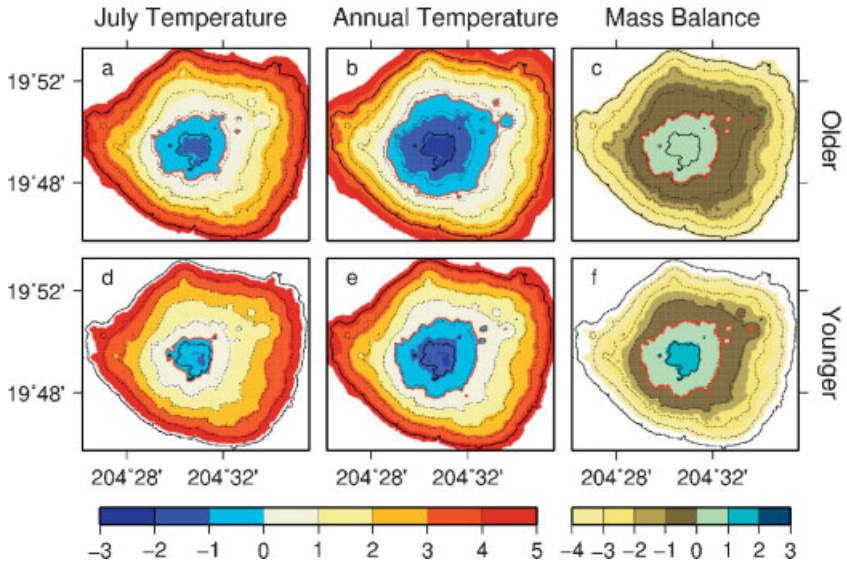

Figure 5 Modelled temperature (July and annual; red lines indicate 0°C) and net mass balance (red lines show ELAS) for the Older Makanaka (a–c) and Younger Makanaka (d–f) glaciations. The units of mass balance are given in m a^{-1}. Topographic contour lines are 1000 m (solid) and 200 m (dashed)

colder than that of Younger Makanaka, and the 0°C isotherms at that time were lower by approximately 120 m. The summit of Mauna Kea had freezing temperatures all year; the minimum annual average temperature was about −3°C and −2°C for the Older and Younger Makanaka, respectively, and the annual/July 0°C isotherms were 3775/3955 m and 3650/3840 m a.s.l. during these glaciations. The net mass balances (Fig. 5(c) and (f)) are correspondingly different: the gradient is steeper for Younger Makanaka; the asymmetry is greater for Older Makanaka; and the maximum is greater for Younger Makanaka. Although the ELAs are essentially the same for the two ice caps, their relationships with temperatures are not. The Younger Makanaka ELA correlates best with the elevation of the 0°C annual isotherm, whereas the Older Makanaka ELA correlates with the elevation of the 0°C July isotherm (Fig. 5), the same as the modern ELA (Fig. 6, Table 2).

Palaeo-ELAs were obtained by finding average elevations of zero mass balance (Fig. 6): 3805 m a.s.l. for Older Makanaka, 3780 m a.s.l. for Younger Makanaka, and 4680 m a.s.l. for today (extrapolated above the summit). These are similar to the palaeo- ELAs of Porter (1979a), but differ from Blard *et al.*'s (2007) present-day altitude of zero mass balance, which they place at ~5400 m a.s.l. Similarly, the 0°C isotherms (annual and July) are 3650 m a.s.l. and 3840 m a.s.l. for Older Makanaka, 3775 m a.s.l. and 3955 m a.s.l. for Younger Makanaka, and 4470 m a.s.l. and 4690 m a.s.l. for today. The observed trend follows the temperature pattern: coldest during Older Makanaka, warmest today.

To quantify glacial-time precipitation rates, SLTs were prescribed using both the pollen and alkenone temperature records, and ice margin elevations were calculated from moraine data. We estimated precipitation using Monte Carlo simulation, in which we generated 1000 precipitation estimates using prescribed ranges of temperature and ice margin elevation (normal distribution was assumed for both variables). Using the pollen record as input, the calculated annual rates of precipitation at 3800 m a.s.l. are 1100 ± 130 mm and

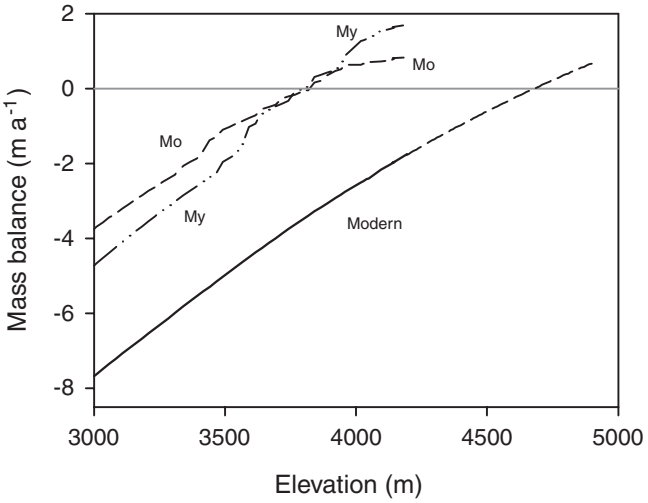

Figure 6 Integrated mass balance and average ELA calculated from the model output shown in Fig. 5. Dashed line, extrapolated above 4200 m a.s.l., represents area above the summit of Mauna Kea

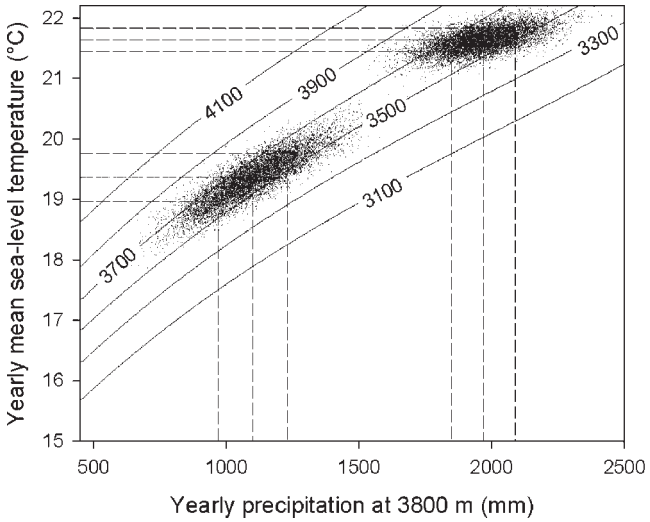

Figure 7 Reconstruction of glacial-time precipitation rates on Mauna Kea at 3800 m a.s.l. Two clusters of 1000 points each were generated using Monte Carlo simulation, with normally distributed temperature and moraine elevation for the Younger Makanaka glaciation (top right cluster; annual precipitation rate of 1970 ± 120 mm) and for the Older Makanaka glaciation (lower left cluster; annual precipitation rate of 1100 ± 130 mm). Ice extent elevation contours are the same as those shown in Fig. 4

DOI: 10.1002/jqs

1970 ± 120 mm for the Older and Younger Makanaka glaciations, respectively (Fig. 7). Calculations using the alkenone-derived SST record as input yield similar results: 1235 ± 145 mm and 1735 ± 95 mm for the Older and Younger Makanaka glaciations, respectively. For reference, the modern annual precipitation at this elevation is 450 mm. Modelling results are summarised in Fig. 7 and Table 2. For these precipitation rates the change in lapse rates between the Younger Makanaka glaciation and present day is $-0.74^{\circ}C\,km^{-1}$ (pollen) and $-0.63^{\circ}C\,km^{-1}$ (alkenone), and between the Older Makanaka glaciation and present day is $-0.32^{\circ}C\,km^{-1}$ (pollen) and $-0.39^{\circ}C\,km^{-1}$ (alkenone). These values are smaller than the change of $-2.0^{\circ}C\,km^{-1}$ to $-2.2^{\circ}C\,km^{-1}$ determined by Farrera *et al.* (1999) between the LGM and today based on the mean temperature of the coldest month from plant and pollen macrofossil records from the Pacific region. Blard *et al.* (2007) estimate the change in lapse rate between glacial and present-day conditions to be $-1.0^{\circ}C\,km^{-1}$.

Changes in lapse rates of these amounts are larger than the maximum seasonal change in present-day lapse rates ($0.4^{\circ}C\,km^{-1}$ between June and March, Fig. 4(b)) and modelled precipitation rates are significantly larger (by a factor of ~2 for the Older Makanaka glaciation and ~4 for Younger Makanaka glaciation) than present-day values. It should be noted therefore that the reconstructions of past climates made here rely on a significant extrapolation of the present-day trend between lapse rates and precipitation, but no alternative method is available.

Finally, we conducted a sensitivity analysis to determine how potential errors in our glacial chronology could affect our high-elevation precipitation estimates for the two Makanaka glaciations (Table 3). Errors in the ^{36}Cl glacial ages are propagated through our model because we extracted low-elevation temperature values from the pollen and alkenone records for the periods that correspond to the ^{36}Cl ages. Our sensitivity analysis assumes that these ^{36}Cl ages are accurate to within $\pm 10\%$. Within this range, the difference in low-elevation air temperatures between the Older and Younger Makanaka glaciations (model input) remains relatively constant at ~1.3°C. The corresponding estimates of high-elevation precipitation (model output) for each glaciation vary by ~100 mm a^{-1} (or <9%) within this range. Thus, if our glacial ages are accurate to within $\pm 10\%$, then our overall conclusions regarding the different causes of the Makanaka glaciations are robust. If our ages are in error beyond this limit, then the difference in the modelled precipitation between the Makanaka glaciations would be reduced. Modelled precipitation during the Older Makanaka would increase because the input temperature would also increase, but modelled precipitation during Younger Makanaka times would remain largely unchanged because air temperatures did not change significantly for several millennia both before and after ~13 ka ago.

Palaeoclimatic interpretations

When snow falls on Mauna Kea today, it rarely lasts more than a few days because of generally positive temperatures and intense solar radiation. The source of high-elevation moisture is usually high-altitude clouds associated with frontal systems emanating from the west, which are common in the winter, and rarely with the trade winds, which prevail in the summer. Trade winds that reach Hawai'i originate from the subtropical high-pressure ridge of the North Pacific anticyclone, located to the north and north-east of the archipelago (Juvik and Juvik, 1998). Low-elevation windward (eastern) slopes receive the most precipitation brought by the trade winds; higher elevations receive progressively less precipitation because moisture is depleted as the air moves up. In addition, a quasi-permanent temperature inversion exists between 1500 and 3000 m a.s.l. (Juvik and Juvik, 1998), locking most of the moisture below ~3000 m a.s.l. Occasionally trade winds do break through the inversion, but do not contribute a significant portion of the annual precipitation to the summit area. In contrast, during winter months, trade winds are more subdued as the subtropical ridge weakens and migrates to the south. This allows tropical storms associated with eastward-moving cold fronts to cross the island chain. These storms are not restricted in elevation like those associated with trade winds and, therefore, they can supply precipitation to the summit area of Mauna Kea.

On multiyear timescales, variability of winter precipitation depends on the strength of the El Niño Southern Oscillation (ENSO) (Yu *et al.*, 1997; Juvik and Juvik, 1998). Trade winds weaken during weak ENSO years, and intensify during strong ENSO years. Consequently, copious winter precipitation is correlated with the La Niña conditions (weak phase of ENSO), and winter droughts are a feature of strong ENSO. Interannual variations can be very large. For example, in the last 30 years, January precipitation in Honolulu (O'ahu) varied from nearly zero during El Niño winters (strong ENSO) to more than 400 mm during La Niña winters (Juvik and Juvik, 1998).

Based on modern climate conditions and our modelling results, we propose that Pleistocene glaciations in Hawai'i were

Table 3 Sensitivity analysis

Age factor	^{36}Cl age (ka, 1σ)	$\Delta T_{463\ m}$ (°C) Pollen	$\Delta T_{463\ m}$ (°C) Alkenone	$T_{0\ m}$ (°C) Pollen	$T_{0\ m}$ (°C) Alkenone	$P_{3800\ m}$ (mm a^{-1}) Pollen	$P_{3800\ m}$ (mm a^{-1}) Alkenone
Younger Makanaka							
×1.0	13.0 ± 0.4	-0.66 ± 0.19	-1.23 ± 0.03	21.64 ± 0.19	21.07 ± 0.03	1970 ± 120	1735 ± 95
×0.9	11.7 ± 0.3	-0.41 ± 0.05	-1.16 ± 0.02	21.89 ± 0.05	21.14 ± 0.02	2070 ± 110	1765 ± 100
×1.1	14.3 ± 0.4	-0.31 ± 0.12	-1.51 ± 0.16	21.99 ± 0.12	20.79 ± 0.16	2115 ± 110	1630 ± 90
Older Makanaka							
×1.0	23.1 ± 1.2	-2.93 ± 0.40	-2.55 ± 0.43	19.37 ± 0.40	19.75 ± 0.43	1100 ± 130	1230 ± 145
×0.9	20.8 ± 1.1	-2.61 ± 0.61	-2.31 ± 0.17	19.69 ± 0.61	19.99 ± 0.17	1220 ± 210	1310 ± 80
×1.1	25.4 ± 1.4	-1.80 ± 1.11	-2.83 ± 0.46	20.50 ± 1.11	19.47 ± 0.46	1510 ± 410	1130 ± 160

Abbreviations for model parameters:

- $\Delta T_{463\ m}$ = difference in temperature between glacial periods and today at an elevation of 463 m (model input)
- $T_{0\ m}$ = air temperature at sea level (model output)
- $P_{3800\ m}$ = annual precipitation at an elevation of 3800 m (model output)

DOI: 10.1002/jqs

caused by the intensification of the high-altitude precipitation associated with mid-latitude storms and cold fronts, and probably not by the intensification of the trade winds or westward-moving tropical cyclones. Two clues point in this direction: the reconstructed precipitation rates and the shapes of the Makanaka ice caps. The analysis of glacial-time precipitation rates at sea level (Hotchkiss and Juvik, 1999) and at mountain altitudes (this work) indicates changes by approximately the same amounts: $\sim 1.5\,m\,a^{-1}$ during Younger Makanaka, and $\sim 0.5\,m\,a^{-1}$ during Older Makanaka. If, as suggested by Porter (1979a, 2005), the enhanced precipitation regime in the Late Pleistocene was due to the intensification of the trade winds or tropical cyclones, lower altitudes would receive more precipitation than mountain altitudes, which is not the case. In contrast, if the increased precipitation was caused by the increased frequency and intensity of the storm tracks and cold fronts passing over the islands, all altitudes would receive approximately the same precipitation, and some of it would be snow, as it is today. This scenario is consistent with our results.

The near-symmetry of the Makanaka ice caps also indicates that trade winds were not the main source of moisture feeding the ice caps. We considered a hypothetical case of a glaciation with the modern (trade-wind-dominated) precipitation pattern intensified by a constant factor, and obtained unreasonable results: the ice cap was strongly asymmetric (~600 m difference in ELA between west and east, whereas the moraine distribution suggests that it should be ~100 m), and the sea-level precipitation was unreasonably high (in excess of $12\,m\,a^{-1}$). Together, these two arguments indicate that the intensification of high-altitude winter precipitation played the leading role in the build-up and maintenance of the Makanaka ice caps, suggesting that the source of moisture for the Makanaka ice caps was in the western Pacific.

Precipitation alone cannot support glaciers if temperatures are too high. Our ^{36}Cl results show that the Older Makanaka glaciation was broadly coincident with the LGM, which, at low elevations in Hawai'i, was characterised by temperatures 2.5–3.0°C lower than modern (Fig. 3) (Hotchkiss and Juvik, 1999; Lee and Slowey, 1999). These are borderline temperatures for glacier development (Fig. 4(a)), and certainly not sufficient to produce ice caps of the Makanaka size. The Younger Makanaka glacial advance occurred at the time when low-elevation temperatures were approximately as warm as today and nearly constant for several millennia (Fig. 3). Under these conditions glaciation would be impossible without unreasonably high precipitation rates (Fig. 4(a)) because snow could never last through the ablation season.

But glaciations did occur, and the question is why snow and ice did not melt. Our analysis of lapse rates suggests that they are inversely correlated with precipitation rates (Fig. 4), and since precipitation rates were higher during both Makanaka times, lapse rates may have been correspondingly steeper. Our precipitation-corrected lapse rates, combined with the low-elevation pollen-based temperature record (Hotchkiss and Juvik, 1999), the alkenone-derived SST record (Lee and Slowey, 1999; Lee *et al.*, 2001) and our own moraine data, yield freezing air temperatures on top of Mauna Kea during both Makanaka glaciations (Table 2). Modelled air temperatures at 3800 m a.s.l. were approximately equal in Younger and Older Makanaka times (Table 2), despite a large difference in near-sea-level temperatures. This convergence of high-elevation temperatures is due to a difference of $+0.42°C\,km^{-1}$ in lapse rates between the Younger and Older Makanaka (Table 2), which, transferred from sea level to an elevation of 3800 m, results in a temperature difference of ~1.6°C. This is similar to the difference between low-elevation temperatures during the Older and Younger Makanaka glaciations (Table 2). Thus, it appears that our adjusted glacial-time lapse rates explain almost entirely the apparent discrepancy between glacial sea-level temperatures with high-altitude estimates derived from glacial–geological data.

Whereas Makanaka temperatures at sea level and high altitudes may be explained adequately, we do not know what caused the precipitation rates to be different during the two glacial episodes. We speculate that atmospheric circulation and moisture transport and delivery to the volcano hold the clues. Atmospheric circulation models and climate records suggest that the position of the high-pressure ridge of the North Pacific anticyclone was shifted to the south during the Late Pleistocene, in part as a response to an eastward shift and expansion of the Aleutian low (COHMAP, 1988; Sabin and Pisias, 1996; Kutzbach *et al.*, 1998). If the magnitude of this shift was similar to the modern summer–winter migration of the high-pressure cell, then trade winds would not have been as strong or persistent (although they still were likely present) and precipitation in the summit area of Mauna Kea would have been higher than modern throughout the year. If, in addition, there were strong millennial-scale changes similar to those that characterise the modern ENSO (El Niño–La Niña), then during palaeo-La Niña times precipitation would be enhanced even more, leading to more snowfall and expansion of ice caps on Mauna Kea. Although somewhat speculative, this scenario seems plausible based on the similar difference in precipitation at low elevations and atop Mauna Kea during the two Makanaka glacial times.

The results presented here underscore the importance of precipitation on tropical glaciers, and thus have broad implications for the understanding of glacial-time glaciers and climate in the tropics. They suggest that precipitation plays a dual role in glacier growth: increasing precipitation provides additional moisture for the glacier accumulation area, and increased moisture makes temperature lapse rates steeper; both factors lead to advance of glaciers. Additional research is needed to determine whether precipitation-dependent lapse rates are limited to Hawai'i, or are common in the tropics. In the latter case, precipitation-dependent lapse rates may possibly reconcile the difference between small cooling at low altitudes and much greater cooling at mountain elevations (e.g. Farrera *et al.*, 1999), and help solve the long-standing problem of inconsistent glacial-time temperature reconstructions based on marine and moraine proxy records.

Summary and conclusions

The youngest glaciations in Hawai'i broadly correlate with stage 2 of the marine isotope record. Cosmogenic ^{36}Cl exposure ages show that the Older Makanaka moraines are 23.1 ± 2.5 ka (2σ) old and the Younger Makanaka deposits are 13.0 ± 0.8 ka old. Despite a difference in low-altitude temperatures of ~2°C between the Younger (warmer) and Older Makanaka, the two ice caps had almost exactly the same lateral extent and similar equilibrium-line altitudes. This apparent inconsistency can be explained by invoking steeper temperature lapse rates and higher precipitation rates during the Younger Makanaka glaciation.

Ice mass balance modelling suggests that in order for an ice cap to exist on top of Mauna Kea atmospheric lapse rates in the past had to be steeper than the modern lapse rates. We have determined that modern lapse rates in Hawai'i correlate with precipitation, and applied this result to the geological past.

DOI: 10.1002/jqs

Lapse rates during glacial times were 0.74°C km^{-1} (Younger Makanaka) and 0.32°C km^{-1} (Older Makanaka) steeper than they are today. These rates reconcile almost all differences between reconstructed SSTs and those reconstructed from lowering of equilibrium line altitudes (ELAs) on Mauna Kea.

Our modelling results indicate that air temperatures on top of Mauna Kea were approximately the same during the two Makanaka times, despite a difference of ~2°C near sea level. The difference almost disappears because of the difference in lapse rates at the two Makanaka times.

Precipitation rates were higher in the past than they are today. Assuming our ^{36}Cl ages are correct, at the elevation of 3800 m precipitation rates were ~2 m a^{-1} (Younger Makanaka) and ~1 m a^{-1} (Older Makanaka), compared to 0.45 m a^{-1} today. The increases of precipitation were approximately the same near sea level (the pollen record) and at mountain altitudes (the glacial record), indicating that precipitation came from high-altitude storm clouds. Today, such clouds are usually associated with frontal systems coming to Hawai'i from the west and not with trade winds.

Our modelling results, combined with present-day climatology, suggest that the Younger Makanaka glaciation was caused by greatly enhanced precipitation under climatic conditions similar to modern La Niña conditions. The Older Makanaka glaciation was probably caused by a combination of slightly enhanced precipitation and slightly colder temperatures with respect to modern.

Makanaka glacial episodes do not appear to correlate directly with glacial deposits of similar ages around the globe. The Older Makanaka terminated by ca. 23 ka, approximately coincident with the LGM, and the Younger Makanaka terminated by 13 ka, near the onset of the Younger Dryas cold event. Thus, ice caps on Mauna Kea were receding at the same time that glaciers elsewhere were at or approaching their maximum extents. If correct, this suggests that glaciers on Mauna Kea did not form solely in response to the build-up of continental ice sheets in the Northern Hemisphere. Rather than responding to these forcing mechanisms, Makanaka ice caps may have responded more directly to changes within the tropical ocean atmosphere system, such as Walker circulation, insolation, seasonality and possibly millennial-scale ENSO-type variations. This implies that other tropical glaciers might also respond to these forcing mechanisms, rather than following expansion and contraction of continental ice sheets. If so, then tropical glacial deposits in general, and those on Mauna Kea in particular, contain palaeoclimatic information that compliments, rather than duplicates, glacial records from higher latitudes.

Acknowledgements We thank E. Wolfe for sharing his knowledge of the geology of Mauna Kea, and for field assistance. We thank K. Quast, D. Desilets and S. Desilets for field assistance. We are grateful to D. Lea, T. Lowell, S. Ivy-Ochs and three anonymous reviewers for providing valuable insights and comments on earlier versions of this manuscript. We also thank S. Porter, L. Owen and an anonymous reviewer for comments and suggestions that greatly improved the final version. The Packard Foundation supported fieldwork, sample preparation and geochemical analyses (Fellowship in Science and Engineering number 951832 to MZ), and PRIME Lab, Purdue University supported ^{36}Cl measurements (under NSF grant number EAR-9809983).

References

Anderson K, Bradley E, Zreda M, Rassbach L, Zweck C, Sheehan E. 2007. ACE: Age Calculation Engine: a design environment for cosmogenic dating techniques. In *Proceedings of the International Conference on Advanced Engineering Computing and Applications in Sciences (ADVCOMP'07)*; 39–48.

Aruscavage PJ, Campbell EY. 1983. An ion-selective electrode method for determination of chlorine in geological materials. *Talanta* **30**: 745–749.

Bevington PR, Robinson DK. 1992. *Data Reduction and Error Analysis for the Physical Sciences*. McGraw-Hill: Boston, MA.

Blard P-H, Lave J, Pik R, Wagnon P, Bourles D. 2007. Persistence of full glacial conditions in the central Pacific until 15 000 years ago. *Nature* **449**: 591–594.

Bond GC, Lotti R. 1995. Iceberg discharges into the North Atlantic on millennial time scales during the last glaciation. *Science* **267**: 1005–1010.

Braithewaite RJ. 1995. Positive degree-day factors for ablation on the Greenland ice sheet studied by energy balance modeling. *Journal of Glaciology* **41**: 153–160.

Cerling TE, Craig H. 1994. Geomorphology and in-situ cosmogenic isotopes. *Annual Review of Earth and Planetary Sciences* **22**: 273–317.

Champion DE. 1980. Holocene geomagnetic secular variation in the western United States: implications for the global geomagnetic field. *U.S. Geological Survey open-file report* 80-824: 1–314.

COHMAP. 1988. Climatic changes of the last 18 000 years: observations and model simulations. *Science* **241**: 1043–1052.

Crowley TJ. 2000. CLIMAP SSTs re-revisited. *Climate Dynamics* **16**: 241–255.

Davis JR, Schaeffer OA. 1955. Chlorine-36 in nature. *Annals of the New York Academy of Science* **62**: 105–122.

Denton GH, Hendy CH. 1994. Younger Dryas Age advance of Franz Josef Glacier in the Southern Alps of New Zealand. *Science* **264**: 1434–1437.

Denton GH, Heusser CJ, Lowell TV, Moreno PI, Anderson BG, Heusser LE, Schluchter C, Marchant DR. 1999. Interhemispheric linkage of paleoclimate during the last glaciation. *Geografiska Annaler* **81A**: 107–152.

Desilets D, Zreda M. 2003. Spatial and temporal distribution of secondary cosmic-ray nucleon intensities and applications to *in-situ* cosmogenic dating. *Earth and Planetary Science Letters* **206**: 21–42.

Desilets D, Zreda M, Almasi PF, Elmore D. 2006. Determination of cosmogenic ^{36}Cl in rocks by isotope dilution: innovations, validation and error propagation. *Chemical Geology* **233**: 185–195.

Diaz HF, Graham NE. 1996. Recent changes in tropical freezing heights and the role of sea surface temperature. *Nature* **383**: 152–155.

Dorn RI, Phillips FM, Zreda MG, Wolfe EW, Jull AJT, Donahue DJ, Kubik P, Sharma P. 1991. Glacial chronology of Mauna Kea, Hawaii, as constrained by surface-exposure dating. *National Geographic Research and Exploration* **7**: 456–471.

Durre I, Vose RS, Wuertz DB. 2006. Overview of the Integrated Global Radiosonde Archive. *Journal of Climate* **19**: 53–68.

Dzierzek J, Zreda M. 2007. Timing and style of deglaciation of north-eastern Poland from cosmogenic ^{36}Cl dating of glacial and glacio-fluvial deposits. *Geological Quarterly* **51**: 203–216.

Fairbanks R. 1989. A 17 000-year glacio-eustatic sea level record: influence of glacial melting rates on the Younger Dryas event and deep-ocean circulation. *Nature* **342**: 637–642.

Farrera I, Harrison SP, Prentice IC, Ramstein G, Guiot J, Bartlein PJ, Bonnefille R, Bush M, Cramer W, von Grafenstein U, Holmgren K, Hooghiemstra H, Hope G, Jolly D, Lauritzen SE, Ono Y, Pinot S, Stute M, Yu G. 1999. Tropical climates at the Last Glacial Maximum: a new synthesis of terrestrial palaeoclimate data. I. Vegetation, lake levels and geochemistry. *Climate Dynamics* **15**: 823–856.

Godsey HS, Currey DR, Chan MA. 2005. New evidence for an extended occupation of the Provo shoreline and implications for regional climate change, Pleistocene Lake Bonneville, Utah, USA. *Quaternary Research* **63**: 212–223.

Gosse JC, Klein J, Evenson EB, Lawn B, Middleton R. 1995. Beryllium-10 dating of the duration and retreat of the last Pinedale glacial sequence. *Science* **268**: 1329–1333.

Guyodo Y, Valet J-P. 1999. Global changes in intensity of the Earth's magnetic field during the past 800 kyr. *Nature* **399**: 249–252.

Hallet B, Putkonen J. 1994. Surface dating of dynamic landforms: young boulders on aging moraines. *Science* **265**: 937–940.

Heinrich H. 1988. Origin and consequences of cyclic ice rafting in the northeast Atlantic Ocean during the past 130 000 years. *Quaternary Research* **29**: 142–152.

Hendy IL, Kennett JP, Roark EB, Ingram BL. 2002. Apparent synchroneity of submillennial scale climate events between Greenland and Santa Barbara Basin, California from 30-10 ka. *Quaternary Science Reviews* **21**: 1167–1184.

Hostetler SW, Clark PU. 2000. Tropical climate at the last glacial maximum inferred from glacier mass-balance modeling. *Science* **290**: 1747–1750.

Hotchkiss S, Juvik JO. 1999. A Late-Quaternary pollen record from Ka'au Crater, O'ahu, Hawaii. *Quaternary Research* **52**: 115–128.

Ivy-Ochs S, Schlüchter C, Kubik PW, Synal HA, Beer J, Kerschner H. 1996. The exposure age of an Egesen moraine at Julier Pass, Switzerland measured with the cosmogenic radionuclides. *Eclogae Geologicae Helvetiae* **89**: 1049–1063.

Juvik SP, Juvik JO. 1998. *Atlas of Hawaii*. University of Hawaii Press: Honolulu.

Kennett JP, Ingram BL. 1995. A 20 000-year record of ocean circulation and climate change from the Santa Barbara Basin. *Nature* **377**: 510–514.

Kutzbach J, Gallimore R, Harrison S, Behling P, Selin R, Laarif F. 1998. Climate and biome simulations for the past 21 000 years. *Quaternary Science Reviews* **17**: 473–506.

Lal D. 1988. In situ-produced cosmogenic isotopes in terrestrial rocks. *Annual Reviews of Earth and Planetary Sciences* **16**: 355–388.

Lea DW, Pak DK, Spero HJ. 2000. Climate impact of Late Quaternary equatorial Pacific sea surface temperature variations. *Science* **289**: 1719–1724.

Lee KE, Slowey NC. 1999. Cool surface waters of the subtropical North Pacific Ocean during the last glacial. *Nature* **397**: 512–514.

Lee KE, Slowey NC, Herbert TD. 2001. Glacial sea surface temperatures in the subtropical North Pacific: a comparison of U^{37}_k, $\delta^{18}O$, and foraminiferal assemblage temperature estimates. *Paleoceanography* **16**: 268–279.

Lowell TV, Heusser CJ, Andersen BG, Moreno PI, Hauser A, Heusser LE, Schluchter C, Marchant DR, Denton GH. 1995. Interhemispheric correlation of Late Pleistocene glacial events. *Science* **269**: 1541–1549.

Mark BG, Harrison SP, Spessa A, New M, Evans DJA, Helmens KF. 2005. Tropical snowline changes at the last glacial maximum: a global assessment. *Quaternary International* **138–139**: 168–201.

Masarik J, Wieler R. 2003. Production rates of cosmogenic nuclides in boulders. *Earth and Planetary Science Letters* **216**: 201–208.

Merrill RT, McElhinny MW, McFadden PL. 1996. *The Magnetic Field of the Earth: Paleomagnetism, the Core, and the Deep Mantle*. Academic Press: London.

Newnham R, Shulmeister J, Singer C, McLea B. 1999. Temperature changes during the Younger Dryas in New Zealand: comment and reply. *Science* **283**: 759.

Oerlemans J. 2001. *Glaciers and Climate Change*. Balkema: Lisse, Netherlands.

Ohno M, Hamano Y. 1992. Geomagnetic poles over the past 10 000 years. *Geophysical Research Letters* **19**: 1715–1718.

Ohno M, Hamano Y. 1993. Global analysis of the geomagnetic-field: time variation of the dipole moment and the geomagnetic pole in the Holocene. *Journal of Geomagnetism and Geoelectricity* **45**: 1455–1466.

Osmaston HA. 2006. Should Quaternary sea-level changes be used to correct glacier ELAs, vegetation belt altitudes and sea level temperatures for inferring climate changes? *Quaternary Research* **65**: 244–251.

Oviatt CG, Nash WP. 1989. Late Pleistocene basaltic ash and volcanic eruptions in the Bonneville basin, Utah. *Geological Society of America Bulletin* **101**: 292–303.

Oviatt CG, Currey DR, Sack D. 1992. Radiocarbon chronology of Lake Bonneville, Eastern Great Basin, USA. *Palaeogeography, Palaeoclimatology, Palaeoecology* **99**: 225–241.

Peng L, King JW. 1992. A late Quaternary geomagnetic secular variation record from Lake Waiau, Hawaii, and the question of the Pacific nondipole low. *Journal of Geophysical Research* **97**: 4407–4424.

Peteet D. 1995. Global Younger Dryas? *Quaternary International* **28**: 93–104.

Phillips FM, Leavy BD, Jannik NO, Elmore D, Kubik PW. 1986. The accumulation of cosmogenic chlorine-36 in rocks: a method for surface exposure dating. *Science* **231**: 41–43.

Phillips FM, Zreda MG, Smith SS, Elmore D, Kubik PW, Sharma P. 1990. A cosmogenic chlorine-36 chronology for glacial deposits at Bloody Canyon, Eastern Sierra Nevada, California. *Science* **248**: 1529–1532.

Phillips FM, Zreda MG, Smith SS, Elmore D, Kubik PW, Dorn RI, Roddy DJ. 1991. Age and geomorphic history of Meteor Crater, Arizona, from cosmogenic ^{36}Cl and ^{14}C in rock varnish. *Geochimica et Cosmochimica Acta* **55**: 2695–2698.

Phillips FM, Zreda MG, Flinsch MR, Elmore D, Sharma P. 1996. A reevaluation of cosmogenic ^{36}Cl production rates in terrestrial rocks. *Geophysical Research Letters* **23**: 949–952.

Phillips FM, Stone WD, Fabryka-Martin JT. 2001. An improved approach to calculating low-energy cosmic-ray neutron fluxes near the land/atmosphere interface. *Chemical Geology* **175**: 689–701.

Pigati JS, Lifton NA. 2004. Geomagnetic effects on time-integrated cosmogenic nuclide production rates with emphasis on ^{14}C and ^{10}Be. *Earth and Planetary Science Letters* **226**: 193–205.

Porter SC. 1979a. Hawaiian glacial ages. *Quaternary Research* **12**: 161–187.

Porter SC. 1979b. Quaternary stratigraphy and chronology of Mauna Kea, Hawaii: a 380 000 year record of mid-Pacific volcanism and ice-cap glaciation: Part II. Complete article. *Geological Society of America Bulletin* **90**: 980–1093.

Porter SC. 1979c. Geologic map of Mauna Kea volcano, Hawai'i. *Geological Society of America Map and Chart Series MC-30*: scale 1:48 000.

Porter SC. 2001. Snowline depression in the tropics during the last glaciation. *Quaternary Science Reviews* **20**: 1067–1091.

Porter SC. 2005. Pleistocene snowlines and glaciation of the Hawaiian Islands. *Quaternary International* **138–139**: 118–128.

Porter SC, Stuiver M, Yang IC. 1977. Chronology of Hawaiian glaciations. *Science* **195**: 61–63.

Reimer PJ, Baillie MGL, Bard E, Bayliss A, Beck JW, Bertrand CJH, Blackwell PG, Buck CE, Burr GS, Cutler KB, Damon PE, Edwards RL, Fairbanks RG, Friedrich M, Guilderson TP, Hogg AG, Hughen KA, Kromer B, McCormac FG, Manning SW, Ramsey CB, Reimer RW, Remmele S, Southon JR, Stuiver M, Talamo S, Taylor FW, van der Plicht J, Weyhenmeyer CE. 2004. IntCal04 terrestrial radiocarbon age calibration, 0–26 cal kyr BP. *Radiocarbon* **46**: 1029–1058.

Sabin AL, Pisias NG. 1996. Sea surface temperature changes in the northeastern Pacific Ocean during the past 20 000 years and their relationship to climate change in North America. *Quaternary Research* **46**: 48–61.

Shackleton NJ. 2000. The 100 000-year ice-age cycle identified and found to lag temperature, carbon dioxide, and orbital eccentricity. *Science* **289**: 1897–1902.

Sharp WD, Turrin BD, Renne PR, Lanphere MA. 1996. $^{40}Ar/^{39}Ar$ and K-Ar dating of lavas from the Hilo 1-km corehole, Hawaii Scientific Drilling Project. *Journal of Geophysical Research* **101**: 11607–11616.

Singer C, Shulmeister J, McLea B. 1998. Evidence against a significant Younger Dryas cooling event in New Zealand. *Science* **281**: 812–814.

Stone JO, Allan GL, Fifield LK, Cresswell RG. 1996. Cosmogenic chlorine-36 from calcium spallation. *Geochimica et Cosmochimica Acta* **60**: 679–692.

Stuiver M, Reimer PJ. 1993. Extended ^{14}C database and revised CALIB radiocarbon calibration program. *Radiocarbon* **35**: 215–230.

Swanson TW, Caffee ML. 2001. Determination of ^{36}Cl production rates derived from the well-dated deglaciation surfaces of Whidbey and Fidalgo Islands, Washington. *Quaternary Research* **56**: 366–382.

Wolfe EW, Wise WS, Dalrymple GB. 1997. The geology and petrology of Mauna Kea Volcano, Hawaii: a study of postshield volcanism. *US Geological Survey Professional Paper* **1557**: 1–129.

Yang S, Odah H, Shaw J. 2000. Variations in the geomagnetic dipole moment over the last 12 000 years. *Geophysical Journal International* **140**: 158–162.

DOI: 10.1002/jqs

Yu Z-P, Chu P-S, Schroeder T. 1997. Predictive skills of seasonal to annual rainfall variations in the US Affiliated Pacific Islands: canonical correlation analysis and multivariate principal component regression approaches. *Journal of Climate* **10**: 2586–2599.

Zreda MG. 1994. Development and calibration of the cosmogenic ^{36}Cl surface exposure dating method and its application to the chronology of Late Quaternary glaciations. PhD thesis, New Mexico Institute of Mining and Technology.

Zreda MG, Phillips FM, Elmore D, Kubik PW, Sharma P, Dorn RI. 1991. Cosmogenic chlorine-36 production rates in terrestrial rocks. *Earth and Planetary Science Letters* **105**: 94–109.

Zreda MG, Phillips FM, Kubik PW, Sharma P, Elmore D. 1993. Eruption age at Lathrop Wells, Nevada from cosmogenic chlorine-36 accumulation. *Geology* **21**: 57–60.

Zreda MG, Phillips FM, Elmore D. 1994. Cosmogenic ^{36}Cl accumulation in unstable landforms. 2. Simulations and measurements on eroding moraines. *Water Resources Research* **30**: 3127–3136.

Zreda M, England J, Phillips F, Elmore D, Sharma P. 1999. Unblocking of the Nares Strait by Greenland and Ellesmere ice-sheet retreat 10 000 years ago. *Nature* **398**: 139–142.

Zreda M, Desilets D, Li Y, Bradley E, Anderson KM. 2005. iCRONUS meets CRONUS-Earth: improved calculations for cosmogenic dating methods – from neutron intensity to previously ignored correction factors. In *15th Goldschmidt Conference*, Moscow, ID.

Appendix A: cosmogenic ^{36}Cl production rates

Cosmogenic ^{36}Cl surface exposure ages were calculated using a new approach that is being implemented in the ACE (formerly iCRONUS) cosmogenic dating software (Anderson *et al.*, 2007) using the following production rates: 71.6 ± 3.8 atoms ^{36}Cl (g Ca)$^{-1}$ a^{-1}, 155.1 ± 9.6 atoms ^{36}Cl (g K)$^{-1}$ a^{-1}, and 676 ± 40 fast neutrons (g air)$^{-1}$ a^{-1} (Fig. A.1). These rates have been scaled to sea level, high geomagnetic latitude using Desilets and Zreda (2003) and modern geomagnetic field conditions (referenced to the 1945.0 Definitive Geomagnetic Reference Field) using Pigati and Lifton (2004); we call them *reference production rates*. These rates are based on the calibration samples of Phillips *et al.* (1990), augmented by high-potassium samples from three additional sources: (1) Ivy-Ochs *et al.* (1996); (2) Zreda *et al.* (1999); and (3) F. M. Phillips (2005, pers. comm.).

Because we dated whole rocks in this study, our samples have all three primary production mechanisms: spallation on K, spallation on Ca, and thermal neutron capture by Cl. Thus, any systematic uncertainties or biases associated with a single production mechanism are largely minimised or even cancelled out. This would not be the case if we had used a specific mineral in which one production mechanism was dominant. The whole-rock chemistry of our samples is similar to the samples in the augmented calibration dataset which we used to calculate production rates for each reaction pathway (Fig. A.2).

Other ^{36}Cl production rate estimates are available (e.g., Stone *et al.*, 1996; Swanson and Caffee, 2001), which would result in different age estimates for the samples. However, we favour our approach for several reasons: (1) ^{36}Cl production rates have been determined using 37 samples of different ages (2 to 49 ka) from 17 separate surfaces at eight locations; other production rates are based on fewer samples and/or fewer localities; (2) ^{36}Cl production rates from all three primary target elements (Cl, K and Ca) have been calculated simultaneously; (3) laboratory procedures used in the production rate estimation and for some of the samples in this research were identical (the open vessel technique); (4) computational procedures used for production rate estimation and for ^{36}Cl age calculations were identical, which assures the compatibility of all results.

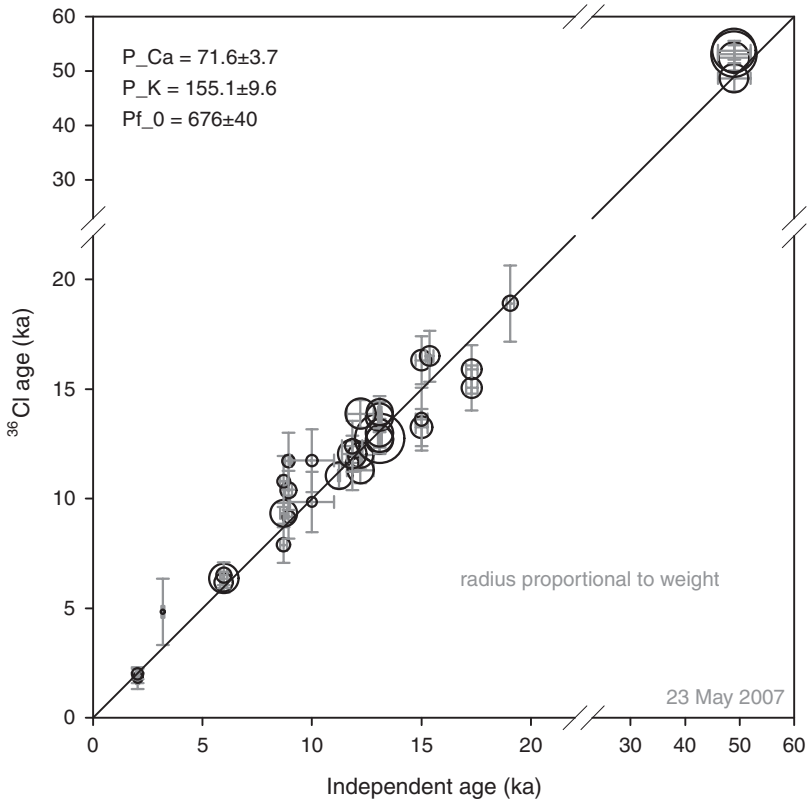

Figure A.1 calibration of the ^{36}Cl geochronometer; comparison of cosmogenic ^{36}Cl ages with independent ages of the calibration samples. P_Ca, production rate due to spallation of Ca; P_K, production rate due to spallation of K; Pf_0, production rate of fast neutrons

DOI: 10.1002/jqs

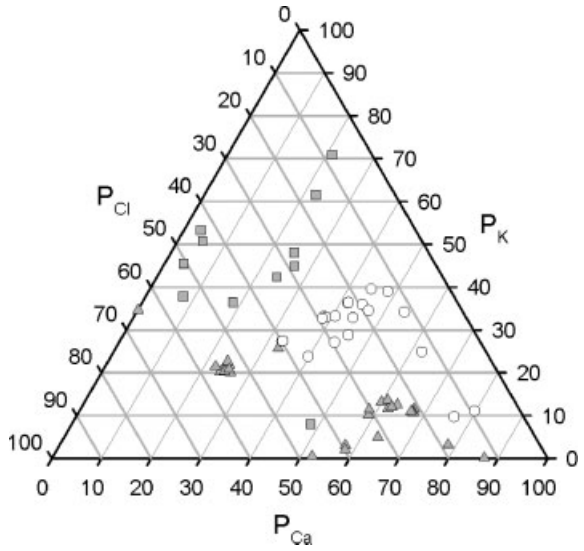

Figure A.2 Percentage of total production rate from Ca, K and Cl for calibration samples (triangles, original data set of Phillips *et al.* (1996); squares, augmented samples of Ivy-Ochs *et al.*, 1996, Zreda *et al.*, 1999, and F. M. Phillips, 2005, pers. comm.; circles, Hawaiian glacial samples (this study)). The Hawaiian glacial samples are within the limits of the area covered by the calibration dataset

Although it is possible that the production rate based on the dataset of Phillips *et al.* (1996) may have a systematic bias, the existence of any bias has not been determined. On the contrary, ^{36}Cl ages obtained so far agree with those determined for the same surfaces using cosmogenic ^{10}Be (Ivy-Ochs *et al.*, 1996), thermoluminescence (Phillips *et al.*, 1991) and radiocarbon dating (Zreda *et al.*, 1999), which implies that any systematic bias should be small – probably no more than a few per cent.

New information supporting the production rates of Anderson *et al.* (2007) comes from the CRONUS-Earth project (started in March 2005), whose goal is to improve production rate estimates. The project generated its first ^{36}Cl calibration dataset using the Tabernacle Hill basalt flow in central Utah (F. M. Phillips, CRONUS-Earth Meeting, Berkeley, 3–4 December 2005). The Tabernacle Hill basalt flow (38.93° N, 247.48° E) is a small, essentially circular basalt flow that erupted into pluvial Lake Bonneville when the lake was at or near its Provo Shoreline level (Oviatt and Nash, 1989; Godsey *et al.*, 2005). The age of the flow is constrained by radiocarbon ages of 14.3 ± 0.1 ^{14}C ka (Beta-23803; Oviatt and Nash, 1989), obtained from dense tufa on the outer margin of the flow, and 14.5 ± 0.1 ^{14}C ka, when the lake drained catastrophically from the Bonneville highstand to the Provo level in the Bonneville Flood (Oviatt *et al.*, 1992). For the CRONUS-Earth project, six samples were processed from this flow and ^{36}Cl exposure ages were calculated using four sets of production rates Phillips *et al.* (1996, 2001), Stone *et al.* (1996), Swanson and Caffee (2001) and the new production rates used here, calculated using the ACE software (Anderson *et al.*, 2007). The results demonstrate that the ACE-calculated production rates performed best in terms of both accuracy and precision (Fig. A.3). We note that these ^{36}Cl results are preliminary and future research will probably result in improved production rate estimates. If so, then the Hawaiian glacial ^{36}Cl exposure ages can be recalculated using Tables 1 and A.1, which contain all the necessary data.

The reference production rates are valid for sea level (atmospheric pressure 1033 g cm^{-2}) and high geomagnetic latitudes (geomagnetic cut-off rigidity <2 GV), and include necessary (universal) corrections for secular changes in palaeomagnetic intensity, changes in the position of the geomagnetic pole and eustatic changes in sea level. Temporal variations in the Earth's geomagnetic field intensity were made using archaeomagnetic data (Yang *et al.*, 2000) and stacked marine cores (Guyodo and Valet, 1999), and the position of the geomagnetic dipole axis using terrestrial sediments (Champion, 1980; Ohno and Hamano, 1992, 1993; Merrill *et al.*, 1996).

The impact of sea-level changes on cosmogenic production was made using global sea-level data (Fairbanks, 1989; Shackleton, 2000). However, following the recent suggestion by Osmaston (2006) that Pleistocene sea-level changes should not be used to correct atmospheric pressure, we also calculated ages without the eustatic correction. The difference between uncorrected and corrected ages is small: near zero at 13 ka and increasing progressively to approximately +1.4% for samples 25 ka old (Table 1). The reference production rates were scaled to the sample sites using Desilets and Zreda (2003) and include additional corrections for environmental factors such as temperature, pressure and lapse rate (Zreda *et al.*, 2005). Corrections were also made for topographic shielding, which we determined by measuring the inclination to the horizon at

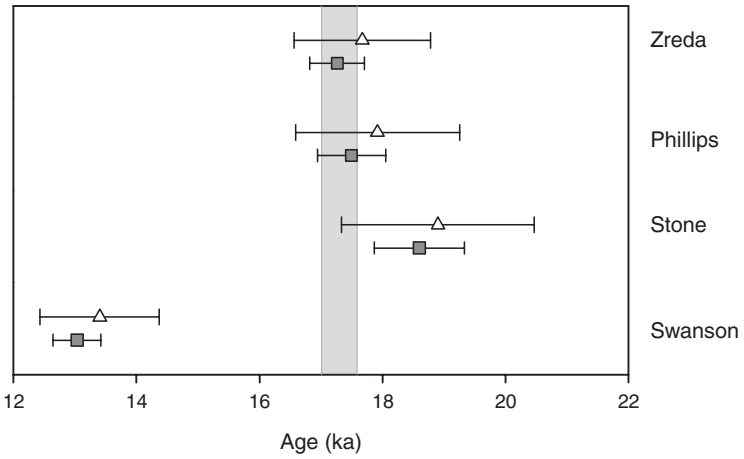

Figure A.3 CRONUS-Earth calibration samples from the Tabernacle Hill basalt flow, central Utah. Independent age of the flow shown by vertical grey bar was determined by ^{14}C on lacustrine tufa (Oviatt and Nash, 1989; Oviatt *et al.*, 1992). Radiocarbon age was converted to calendar years using Calib v. 5.0 (Stuiver and Reimer, 1993; Reimer *et al.*, 2004). Data points represent the mean age of all six samples (triangles) and four 'best' samples

DOI: 10.1002/jqs

Table A.1 Analytical results for latest Mauna Kea glacial landforms

Sample ID	Na_2O (%)	MgO (%)	Al_2O_3 (%)	SiO_2 (%)	P_2O_5 (%)	K_2O (%)	CaO (%)	TiO_2 (%)	MnO (%)	Fe_2O_3 (%)	LOI[a] (%)	Total (%)	B (ppm)	Sm (ppm)	Gd (ppm)	U (ppm)	Th (ppm)	$^{36}Cl/(10^{15}Cl)$	Cl (ppm)
Older Makanaka moraine																			
MK03-05-MKO	4.70	3.17	16.52	51.34	0.45	1.99	5.66	2.20	0.19	11.11	1.65	98.97	5.9	11.8	9.9	1.4	4.1	643 ± 31	173.6 ± 0.1
MK03-04-MKO	5.06	3.23	16.90	52.21	0.90	2.17	5.96	2.24	0.20	10.32	0.77	99.96	11.2	13.5	11.2	1.5	4.5	935 ± 61	78.2 ± 0.1
MK03-06-MKO	4.99	2.98	16.61	52.80	0.65	2.09	5.68	2.23	0.19	10.24	1.36	99.83	5.7	10.6	9.0	1.5	4.6	678 ± 42	123.0 ± 0.3
Outwash channel																			
HI00-32-MA	4.56	4.24	16.44	49.94	0.41	1.80	6.74	2.90	0.20	11.31	0.10	98.65	6.0	11.8	10.6	1.8	5.5	628 ± 17	92.9 ± 1.7
HI00-33-MA	4.53	4.27	16.53	50.52	0.55	1.82	6.82	3.01	0.20	12.09	-0.25	100.09	b.d.	11.9	10.5	1.6	5.3	1,370 ± 60	32.0 ± 0.8
Younger Makanaka moraine																			
MK03-03-My1	4.93	3.34	17.02	52.04	0.60	2.09	6.06	2.51	0.20	10.62	0.42	99.84	1.4	10.6	9.1	1.3	3.7	475 ± 26	95.5 ± 0.2
MK03-19-My2	4.82	3.32	16.94	51.55	0.79	2.13	6.05	2.48	0.20	10.74	0.64	99.67	8.9	12.5	10.6	1.5	4.5	285 ± 20	199.0 ± 0.1
MK03-02-My1	3.76	4.52	14.40	49.09	0.41	1.46	8.66	4.06	0.19	14.06	-0.30	100.31	4.8	7.8	7.2	0.9	3.1	834 ± 42	49.9 ± 0.1
MK03-20-My2	4.92	3.43	16.74	51.50	0.77	2.20	5.91	2.28	0.20	10.08	0.75	98.77	4.9	12.7	11.0	1.6	4.8	693 ± 42	54.9 ± 0.1
MK03-01-My1	4.97	3.34	16.85	53.25	0.53	1.98	5.82	2.45	0.20	10.48	0.51	100.38	b.d.	9.7	8.4	1.3	3.8	886 ± 50	38.7 ± 0.1
MK03-21-My2	5.12	3.08	17.07	51.88	0.64	2.10	5.88	2.39	0.19	10.49	1.15	99.97	6.9	10.4	8.8	1.5	4.4	321 ± 29	112.2 ± 0.1
Meltwater fan																			
MK03-08-BF	2.67	5.74	14.27	46.97	0.26	0.59	10.02	3.68	0.20	14.94	0.32	99.65	1.1	4.6	4.6	0.4	1.8	2,477 ± 87	28.0 ± 0.1
MK03-10-BF	4.47	4.12	16.39	49.01	0.81	1.79	6.82	2.84	0.19	11.30	0.40	98.12	1.6	12.7	10.7	1.2	3.4	381 ± 16	123.8 ± 0.1
MK03-11-BF	4.74	3.85	16.51	51.33	0.55	1.95	6.25	2.80	0.20	11.34	0.29	99.81	3.2	9.7	8.3	1.3	3.9	476 ± 23	79.7 ± 0.1
HI00-27-MA	4.84	3.40	16.92	53.26	0.35	2.08	5.77	2.51	0.19	10.70	0.32	100.33	10.0	7.5	7.0	1.6	4.3	360 ± 23	110.3 ± 2.5
HI00-26-MA	4.97	3.59	16.99	53.38	0.17	2.08	5.64	2.54	0.19	10.74	0.12	100.40	7.0	5.6	4.9	1.5	3.9	451 ± 21	68.0 ± 1.7
MK03-07-BF	4.75	3.63	16.72	51.30	0.47	2.04	6.02	2.72	0.20	12.11	0.18	100.11	7.3	10.4	8.8	1.2	3.7	431 ± 24	71.6 ± 0.3
MK03-09-BF	4.68	3.97	16.41	51.64	0.58	1.97	6.30	2.88	0.21	11.64	0.03	100.30	5.7	10.2	8.8	1.5	3.8	447 ± 19	67.1 ± 0.1
MK03-12-BF	4.51	4.29	16.51	49.00	0.85	1.76	6.99	2.87	0.19	11.54	0.64	99.15	5.8	12.8	11.1	1.2	3.5	212 ± 14	184.2 ± 0.1
Incised bedrock																			
HAW03-9-MK	2.63	5.80	14.61	46.48	0.10	0.57	10.61	3.60	0.19	14.74	N/A	99.33	0.5	13.9	11.9	3.2	9.7	307 ± 14	47.7 ± 2.4

[a] LOI, loss on ignition. Negative numbers indicate an increase in mass (e.g. oxidation of Fe^{2+} to Fe^{3+}).
b.d., below detection limit.

30° azimuthal increments using a hand-held clinometer; the corrections were smaller than 0.2%, except the incised bedrock sample (HAW03-9-IB), for which the correction was 8.8%. Snow cover was found to have a negligible effect on cosmogenic production and no correction for snow cover was applied.

Appendix B: field notes

Older Makanaka moraine

- *Sample MK03-5-Mo*. Collected 24 January 2003. Massive hawaiite boulder on flat surface between two low ridges. Boulder has subrounded edges; no evidence of ventifaction. $1.5 \times 0.8 \times 0.6$ m ($l \times w \times h$). Sampled from top surface, close to the edge, where boulder was least eroded. Yielded ^{36}Cl age of 25.2 ± 2.5 ka (2σ).
- *Sample MK03-4-Mo*. Collected 24 January 2003. Hawaiite boulder on flat surface characterised by matrix of cobbles (>60%) and gravels (20–30%). Boulder has subrounded edges; no evidence of ventifaction. $1.0 \times 1.0 \times 0.6$ m. Sampled from top surface on exposed slope of ~30°. Yielded ^{36}Cl age of 21.7 ± 2.7 ka.
- *Sample MK03-6-Mo*. Collected 24 January 2003. Hawaiite boulder on locally flat terrain with nearby slope of less than 5–10°. Flat, wide boulder; $1.5 \times 1.5 \times 0.7$ m. Sampled from subhorizontal top surface. Yielded ^{36}Cl age of 21.6 ± 2.9 ka.

Outwash channel

- *Sample HI00-32-OC*. Collected 8 April 2000. Massive, hard hawaiite boulder; well-rounded edges; some evidence of ventifaction on NE side; $1.0 \times 1.0 \times 1.0$ m. Sampled from subhorizontal top surface away from ventifaction. Yielded ^{36}Cl age of 20.4 ± 1.4 ka.
- *Sample HI00-33-OC*. Collected 8 April 2000. Outwash boulder from Makanaka till. Massive hard hawaiite; well-rounded edges; evidence of ventifaction on W and NE side; $1.0 \times 0.75 \times 0.75$ m. Weathered light brown to grey. Sampled top of boulder away from ventifaction. Yielded ^{36}Cl age of 18.8 ± 1.9 ka.

Younger Makanaka moraine

- *Sample MK03-3-My1*. Collected 24 January 2003. Good large subrounded boulder on flat part of ridge. No evidence of spalling or ventifaction. $1.5 \times 1.2 \times 0.9$ m. Sampled subhorizontal surface on top of boulder. Yielded ^{36}Cl age of 13.7 ± 1.5 ka.
- *Sample MK03-2-My1*. Collected 24 January 2003. Boulder on locally flat part of ridge. Well-rounded vesicular hawaiite; no evidence of spalling. $1.3 \times 1.0 \times 0.5$ m. Sampled subhorizontal surface on top of boulder. Yielded ^{36}Cl age of 13.6 ± 1.4 ka.
- *Sample MK03-19-My2*. Collected 29 January 2003. Well-rounded vesicular hawaiite; no evidence of spalling; deeply rooted in matrix. $1.5 \times 1.0 \times 0.4$ m. Sampled subhorizontal surface on top of boulder. Yielded ^{36}Cl age of 13.4 ± 1.9 ka.
- *Sample MK03-20-My2*. Collected 29 January 2003. Boulder on flat-topped ridge crest; rounded edges; no evidence of spalling; matrix on SE side of boulder recently deflated ~5–10 cm. $1.2 \times 1.2 \times 0.5$ m. Sampled subhorizontal surface on top of boulder. Yielded ^{36}Cl age of 12.9 ± 1.6 ka.
- *Sample MK03-1-My1*. Collected 24 January 2003. Boulder on ridge in area that is locally flat; no evidence of ventifaction or spalling. Boulder smooth with subrounded edges. $0.8 \times 0.5 \times 0.5$ m. Sampled subhorizontal surface on top of boulder. Yielded ^{36}Cl age of 12.9 ± 1.5 ka.
- *Sample MK03-21-My2*. Collected 29 January 2003. Rounded, varnished boulder on flat area on ridge crest. Evidence of possible spalling on W side of boulder where varnish is disturbed; stayed away from this when sampling. $1.2 \times 1.0 \times 0.6$ m. Sampled subhorizontal surface on top of boulder. Yielded ^{36}Cl age of 10.8 ± 2.0 ka.

Boulder fan

- *Sample MK03-8-BF*. Collected 27 January 2003. Boulder with wide base, no evidence of erosion or spalling; little build-up of sediment around base. $1.2 \times 0.6 \times 0.5$ m. Sampled subhorizontal surface on top of boulder. Yielded ^{36}Cl age of 23.6 ± 1.7 ka.
- *Sample MK03-10-BF*. Collected 27 January 2003. Wide hawaiite boulder with rounded edges; largest boulder in surrounding area. Extremely hard, massive. No evidence of erosion or spalling. $1.5 \times 1.2 \times 0.6$ m. Sampled subhorizontal surface on top of boulder. Yielded ^{36}Cl age of 14.1 ± 1.2 ka.
- *Sample MK03-11-BF*. Collected 27 January 2003. Massive hawaiite boulder with subrounded to subangular edges and wide base that is located on gentle side slope (<5°) of swale. No evidence of spalling or erosion. $1.5 \times 0.9 \times 0.6$ m. Sampled subhorizontal surface on top of boulder. Yielded ^{36}Cl age of 12.9 ± 1.3 ka.
- *Sample HI00-27-BF*. Collected 8 April 2000. Massive hawaiite boulder on levee ~60 cm above active channel. Subrounded edges; wide base. Did not record boulder size. Sampled subhorizontal surface on top of boulder. Yielded ^{36}Cl age of 12.7 ± 1.8 ka.
- *Sample HI00-26-BF*. Collected 8 April 2000. Massive hawaiite boulder ~30 cm above active channel. Subrounded edges; wide base. Did not record boulder size. Sampled subhorizontal surface on top of boulder. Yielded ^{36}Cl age of 11.3 ± 1.2 ka.
- *Sample MK03-7-BF*. Collected 27 January 2003. Massive, vesicular hawaiite boulder. Large boulder with subrounded to subangular edges; wide base. No evidence of spalling or ventifaction. $1.0 \times 0.6 \times 0.4$ m. Sampled subhorizontal surface on top of boulder. Yielded ^{36}Cl age of 11.1 ± 1.3 ka.
- *Sample MK03-9-BF*. Collected 27 January 2003. Large, vesicular boulder with rounded edges on gentle swale ~1–2 m above active channel. Evidence of possible spalling down low on the boulder away from sampled area. $1.2 \times 1.2 \times 1.2$ m. Sampled subhorizontal surface on top of boulder. Yielded ^{36}Cl age of 10.9 ± 0.9 ka.
- *Sample MK03-12-BF*. Collected 27 January 2003. Large rounded boulder with wide base. No evidence of spalling or erosion, but some cracks are apparent. Located on gentle swale ~1–2 m above active channel. $1.5 \times 0.8 \times 0.5$ m. Sampled subhorizontal surface on top of boulder. Yielded ^{36}Cl age of 10.7 ± 1.5 ka.

Incised bedrock

- *Sample HAW03-9-IB*. Collected on 25 April 2003. Volcanic bedrock sampled from a flat surface at the bottom of a 7 m deep incision on the south flank of the volcano. The sampled bedrock was scoured to a smooth polish. Yielded ^{36}Cl age of 13.2 ± 1.9 ka.

DOI: 10.1002/jqs